Comput Mech (2012) 49:545–564
DOI 10.1007/s00466-011-0659-5

ORIGINAL PAPER

A new semi-implicit formulation for multiple-surface flow rules in multiplicative plasticity

P. Areias · D. Dias-da-Costa · E. B. Pires · J. Infante Barbosa

Received: 8 July 2011 / Accepted: 26 October 2011 / Published online: 13 November 2011

Abstract We derive the equations of the multiplicative decomposition in the context of finite strain plasticity with elastic isotropy and arbitrary (isotropic and anisotropic) flow rules. We include multiple surface yield criteria and mixed control of stress components, a requirement for special stress states such as plane stress or uniaxial stress. Ductile damage and fracture are also considered. The approach is also appropriate for symmetric single-crystal flow rules. A direct integration of the rate equations is performed as well as smoothing of the complementarity conditions with the Chen-Mangasarian function. The resulting problem is smooth and always converges quadratically, typically requiring fewer steps than return-mapping algorithms. Exceptional robustness is observed. Illustrative examples are shown in 2D, shells and 3D analyses confirming the combination as very effective for the class of problems considered.

Keywords Finite strain plasticity · Multiplicative decomposition · Multiple yield surfaces · Ductile fractures

P. Areias (✉) · J. I. Barbosa
Departamento de Física, Universidade de Évora,
Colégio Luís António Verney, Rua Romão Ramalho, 59,
7002-554 Evora, Portugal
URL: http://evunix.uevora.pt/~pmaa/
e-mail: pmaa@uevora.pt; pareias@civil.ist.utl.pt

P. Areias
ICIST, Lisbon, Portugal

D. Dias-da-Costa
INESC Coimbra, Department of Civil Engineering,
University of Coimbra, 3030-788 Coimbra, Portugal

E. B. Pires
Departamento de Engenharia Civil e Arquitectura, Instituto
Superior Técnico, Av. Rovisco Pais, 1049-001 Lisbon, Portugal

1 Introduction

Combination of the return-mapping technique [36,50,60] and mixed formulations [18,19] led to a standardization of elasto-plastic modeling with finite elements (see the treatise by Belytschko et al. [15] and the one by Bonet [17]). However, return-mapping algorithms still pose challenges to systematization: the predictor in the presence of ductile damage evolution can give a false indication and there is an implicit inequality for the plastic multiplier. Another problem for implicit return-mapping occurs when the hardening law depends on the plastic strain rate, such as the Johnson-Cook model and Nemat-Nasser models [50]: plastic strain rate may raise the yield stress and produce fictitious unloading. Classical finite strain constitutive approaches (e.g. the rotated $\boldsymbol{F}_e\boldsymbol{F}_p$ method [4]) inherit some of the difficulties of the small strain algorithms.

Besides these problems, in complex simulations the convergence radius is often not satisfactory [25]. For ductile fracture problems, where mesh adaptation, quadrature point alterations and even full remeshing has to be adopted, small convergence radius can be impairing for a successful analysis. Here, we introduce a new finite strain elasto-plastic algorithm able to include, in the same underlying framework, kinematic hardening, anisotropy and damage. Adding to this, recent ductile damage models (specifically the one by Areias et al. [12]) make use of non-differentiable convex yield functions, not easily tractable by classical return-mapping algorithms.

Concerning small strain constitutive implementations, solutions based on the dual formulation are now established both with predictor/corrector [36] and Shur-based methodologies [40]. Our approach consists in smoothing the complementarity condition (cf. [23]) and solving monolithically the resulting system by a classical Newton root finder. Numerous

manuscripts have dealt with J_2 [28,35,58] plasticity in finite strains including kinematic hardening. Cost-effective algorithms are then adopted for von-Mises plasticity, based on radial-return technique (parallel trial elastic strain and final deviatoric stress [36]) which reduces the constitutive solution to one algebraic equation. Of course for finite strains the additional condition of coaxiality of the strain measures and the Kirchhoff stress is either verified or imposed. This started with the paper by Weber and Anand [63]. Semi-implicit methods, which freeze the flow vector in the solution, hence retaining the advantages of the Key and Krieg approach for more complex cases, have been disseminated by Moran et al. (see, e.g. [49]). Other yield functions require the direct use of Lee's decomposition [41] and monolithic integration. This has been done for a similar case by Lührs et al. [45] and it was applied to the von-Mises yield criterion. The lack of smoothness of the problem is still not tackled consistently for this case. We first enumerate our requirements:

- Use of isotropic hyperelastic laws: $\boldsymbol{\tau} \equiv \boldsymbol{\tau}(\boldsymbol{b}_e)$ where $\boldsymbol{b}_e$ is the *elastic* left Cauchy-Green tensor and $\boldsymbol{\tau}$ is the Kirchhoff stress measure (cf. [21, p. 142] for the isotropy limitation).
- Possibility of imposing additional conditions, such as known stress components, in the constitutive system.
- Multiple-surface plasticity, with no restriction in the form of the flow rule or the yield functions.

This work is specially dedicated to the presentation and verification of this new approach for finite strain plasticity. Isoerror maps in finite strains are shown with better results than Simo's classical $\boldsymbol{F}_e\boldsymbol{F}_p$ algorithms ([56–58]). In addition, demanding tests are also performed. Specifically, besides the well known tension test (here performed in 3D) which caused convergence problems in the past (cf. [25]), we also test anisotropic problems, ductile damage and fracture. In addition, in contrast with recent works accounting for elastic anisotropy (specifically [20]) the overall computations are simpler despite the limitation to *elastic* isotropy (plastic anisotropy is of course accounted for).

2 Constitutive model

2.1 Introduction to multiple-surface finite strain plasticity with *elastic* isotropy

The deformation map of a continuous medium is characterized by its derivative, the deformation gradient $\boldsymbol{F}$. For an isotropic hyperelastic material it is known that the Kirchhoff stress can be determined from the left Cauchy-Green tensor, $\boldsymbol{b}$,[1] as (cf. [17,21, p. 162]):

$$\boldsymbol{\tau} = 2\frac{\mathrm{d}\psi_b}{\mathrm{d}\boldsymbol{b}}\boldsymbol{b} = 2\boldsymbol{b}\frac{\mathrm{d}\psi_b}{\mathrm{d}\boldsymbol{b}} \tag{1}$$

where ψ_b is a function of $\boldsymbol{b}$ whose image is the value of the strain energy density.[2] This form of calculating the Kirchhoff stress from the kinematics is specially convenient for computations since Voigt notation can be used ($\boldsymbol{\tau}$ and $\boldsymbol{b}_e$ are symmetric) with considerable savings. In the subsequent sections, we will require the derivative of $\boldsymbol{\tau}$ with respect to $\boldsymbol{F}$. Using (1), the derivative of $\boldsymbol{\tau}$ with respect to $\boldsymbol{F}$ is obtained by the chain rule[3]:

$$\frac{\mathrm{d}\boldsymbol{\tau}}{\mathrm{d}\boldsymbol{F}} = \frac{\partial\boldsymbol{\tau}}{\partial\boldsymbol{b}} : \frac{\mathrm{d}\boldsymbol{b}}{\mathrm{d}\boldsymbol{F}} \tag{2}$$

with the last term being given, in *elasticity*, by its components as:

$$\frac{[\mathrm{d}\boldsymbol{b}]_{ij}}{[\mathrm{d}\boldsymbol{F}]_{mn}} = \delta_{im}\,[\boldsymbol{F}]_{jl} + \delta_{jm}\,[\boldsymbol{F}]_{in} \tag{3}$$

with $i, j, m, n \in \mathscr{I}_{sd}$. The index-set $\mathscr{I}_{sd}$ contains natural numbers up to the number of space dimensions (sd) of the model under consideration. The left-hand-side of (3) is a fourth-order tensor with minor-symmetry in the first and second indices. The classical spatial modulus,[4] can be obtained as:

$$[\mathscr{C}]_{ijkl} = \frac{[\mathrm{d}\boldsymbol{\tau}]_{ij}}{[\mathrm{d}\boldsymbol{F}]_{kn}}\,[\boldsymbol{F}]_{ln} - [\boldsymbol{\tau}]_{il}\,\delta_{jk} - [\boldsymbol{\tau}]_{jl}\,\delta_{ik} \tag{4}$$

This form of $\mathscr{C}$ is deduced by writing the time-derivative of the Kirchhoff stress as in Simo and Hughes [60, p. 255, Eq. 7.1.74]:

$$\mathscr{L}_{\dot{\boldsymbol{x}}}\boldsymbol{\tau} = \dot{\boldsymbol{\tau}} - \boldsymbol{l}\boldsymbol{\tau} - \boldsymbol{\tau}\boldsymbol{l}^T \tag{5}$$

where $\boldsymbol{l} = \dot{\boldsymbol{F}}\boldsymbol{F}^{-1}$ is the spatial velocity gradient and $\mathscr{L}_{\dot{\boldsymbol{x}}}$ is the Lie derivative of $\boldsymbol{\tau}$ using the spatial velocity $\dot{\boldsymbol{x}}$ as the flow. After replacing it, in (5), by the contraction of the spatial modulus with the strain rate (Ref. [60, p. 257, Eq. 7.1.85]) and taking into account minor-symmetry of $\mathscr{C}$, it results:

$$\mathscr{C} : \boldsymbol{l} = \dot{\boldsymbol{\tau}} - \boldsymbol{l}\boldsymbol{\tau} - \boldsymbol{\tau}\boldsymbol{l}^T \tag{6}$$

The time-derivative of the Kirchhoff stress (replacing the left-hand-side of [62] (45.17)) is calculated using the chain rule:

$$[\dot{\boldsymbol{\tau}}]_{ij} = \frac{[\mathrm{d}\boldsymbol{\tau}]_{ij}}{[\mathrm{d}\boldsymbol{F}]_{kn}}\left[\dot{\boldsymbol{F}}\right]_{kn} \tag{7}$$

[1] In the elasticity context, $\boldsymbol{b}_e$ is simply denoted $\boldsymbol{b}$.

[2] Strain energy per unit *undeformed* volume.

[3] To avoid symbol duplication, we use the same symbols for function names and their image.

[4] This is adopted in many finite strain applications due to the sparsity of the initial stress matrix, cf. [14,62].

using the relation $\dot{\boldsymbol{F}} = \boldsymbol{l}\boldsymbol{F}$, we can write (6) for all $\boldsymbol{l}$ as

$$[\mathscr{C}]_{ijkl}\,[\boldsymbol{l}]_{kl} = \frac{[\mathrm{d}\boldsymbol{\tau}]_{ij}}{[\mathrm{d}\boldsymbol{F}]_{kn}}\,[\boldsymbol{l}]_{kl}\,[\boldsymbol{F}]_{ln} - [\boldsymbol{\tau}]_{lj}\,[\boldsymbol{l}]_{il} - [\boldsymbol{\tau}]_{il}\,[\boldsymbol{l}]_{jl} \tag{8}$$

with k, l and n as free-indices. Now we can take the derivative of both members of (8) with respect to $[\boldsymbol{l}]_{kl}$ and obtain the result (4).

The Kirchhoff stress is not classically written in terms of $\boldsymbol{b}$, rather in terms of invariants or principal stretches (see, e.g. [33]). However, to suit our purposes, we write the relevant expressions in terms of $\boldsymbol{b}$. The numerical usefulness of (3) is apparent for finite strain plasticity, since the derivative with respect to an *elastic* left-Cauchy-Green tensor $\boldsymbol{b}_e$ will then have to be related to $\mathscr{C}$ to be used in what is now the classical finite-strain weak form of equilibrium ([58,59,61]) for finite element applications. Note that, given a specific form of ψ_b, any *isotropic* elastic law can be inserted in (1), its derivative calculated and then both $\boldsymbol{\tau}$ and $\mathscr{C}$ are completely defined. Additional kinematical-like internal variables $\boldsymbol{v}$ are also used in the list of ingredients to represent work-hardening phenomena. If normality is assumed, which *implies* convexity of the yield surface, the general constitutive laws for elastic isotropy can be written as:

$$\phi_i \leq 0 \tag{9}$$

$$\phi_i \dot{\gamma}_i = 0 \tag{10}$$

$$\dot{\gamma}_i \geq 0 \tag{11}$$

$$\boldsymbol{F} = \boldsymbol{F}_e \boldsymbol{F}_p \tag{12}$$

$$\boldsymbol{d}_p = \sum_{i=1}^{n_s} \dot{\gamma}_i \boldsymbol{n}_i \tag{13}$$

$$\boldsymbol{d} = \boldsymbol{d}_e + \boldsymbol{d}_p \tag{14}$$

$$\boldsymbol{\tau} = 2\frac{\mathrm{d}\psi_b}{\mathrm{d}\boldsymbol{b}_e}\boldsymbol{b}_e = 2\boldsymbol{b}_e\frac{\mathrm{d}\psi_b}{\mathrm{d}\boldsymbol{b}_e} \tag{15}$$

$$\dot{\boldsymbol{v}} = -\sum_{i=1}^{n_s} \dot{\gamma}_i \boldsymbol{\varphi}_i \tag{16}$$

where

- $\phi_i, \quad i = 1, \ldots, n_s$ are yield functions of a given yield criterion with n_s yield functions. They are given by a difference between an equivalent stress, σ_{eq_i} and a hardening function y : $\phi_i = \sigma_{eq_i} - y$.
- $\dot{\gamma}_i, \quad i = 1, \ldots, n_s$ are the plastic multipliers corresponding to each of the n_s yield functions.
- $\boldsymbol{F}_e$ and $\boldsymbol{F}_p$ are the elastic and plastic parts of the deformation gradient, respectively, as proposed by Lee [41].
- $\boldsymbol{d}_p$ is the plastic strain rate, defined below for the case of elastic isotropy, related to the total strain rate $\boldsymbol{d}$ as in Eq. 14 and $\boldsymbol{d}_e$ is the elastic strain rate. These will be later specified.
- $\boldsymbol{n}_i$ are flow vectors for each of the n_s yield functions.
- $\boldsymbol{b}_e$ is the elastic Cauchy-Green tensor, which measures the recoverable part of the left-Cauchy-Green tensor.
- $\boldsymbol{\varphi}_i$ are n_h-dimensional functions of hardening rates, necessary to represent work-hardening, damage, etc.

The relation between $\boldsymbol{b}_e$ and $\boldsymbol{F}_e$ follows classical conventions (cf. [58]): $\boldsymbol{b}_e = \boldsymbol{F}_e\boldsymbol{F}_e^T = \boldsymbol{F}\boldsymbol{C}_p^{-1}\boldsymbol{F}^T$ and poses no special problems. In contrast, the definition of $\boldsymbol{d}_p$ and therefore the determination of the evolution law for $\boldsymbol{b}_e$ is less direct and is motivated by the equality $\boldsymbol{b}_e^{-1}\boldsymbol{\tau} = \boldsymbol{\tau}\boldsymbol{b}_e^{-1}$ valid for elastic isotropic materials. For isotropic hyperelastic laws we can relate $\boldsymbol{d}_p$ with the time-derivative of $\boldsymbol{b}_e$ assuming a constant $\boldsymbol{F}$. Since $\boldsymbol{b}_e$ depends both on $\boldsymbol{F}_p$ and $\boldsymbol{F}$ we can therefore partition the time increment of $\boldsymbol{b}_e$ in two parts (this is standard, cf. [17]):

$$\dot{\boldsymbol{b}}_e = \underbrace{\frac{\partial \boldsymbol{b}_e}{\partial \boldsymbol{F}} : \dot{\boldsymbol{F}}}_{\overset{\circ}{\boldsymbol{b}}_e} + \underbrace{\frac{\partial \boldsymbol{b}_e}{\partial \boldsymbol{F}_p} : \dot{\boldsymbol{F}}_p}_{\overset{\star}{\boldsymbol{b}}_e} \tag{17}$$

where $\overset{\circ}{\boldsymbol{b}}_e = \dot{\boldsymbol{F}}\boldsymbol{C}_p^{-1}\boldsymbol{F}^T + \boldsymbol{F}\boldsymbol{C}_p^{-1}\dot{\boldsymbol{F}}^T$ is the time-derivative of $\boldsymbol{b}_e$ *assuming* that $\boldsymbol{F}_p$ is constant and $\overset{\star}{\boldsymbol{b}}_e = \boldsymbol{F}\dot{\overline{\boldsymbol{C}_p^{-1}}}\boldsymbol{F}^T$ is the time-derivative of $\boldsymbol{b}_e$ *assuming* that $\boldsymbol{F}$ is constant. Power conjugacy for elastically isotropic materials ($\psi_b \equiv \psi_b(\boldsymbol{b}_e)$) can be written as[5]:

$$\begin{aligned}\dot{\psi}_b &= \frac{\mathrm{d}\psi_b}{\mathrm{d}\boldsymbol{b}_e} : \dot{\boldsymbol{b}}_e = \frac{1}{2}(\boldsymbol{\tau}\boldsymbol{b}_e^{-1}) : \dot{\boldsymbol{b}}_e = \frac{1}{2}\boldsymbol{\tau} : (\dot{\boldsymbol{b}}_e\boldsymbol{b}_e^{-1}) \\ &= \frac{1}{2}(\boldsymbol{b}_e^{-1}\boldsymbol{\tau}) : \dot{\boldsymbol{b}}_e = \frac{1}{2}\boldsymbol{\tau} : (\boldsymbol{b}_e^{-1}\dot{\boldsymbol{b}}_e)\end{aligned} \tag{18}$$

This decomposition is shown, for example, in [17] and its validity is limited to *elastic isotropy*.

Having $\overset{\star}{\boldsymbol{b}}_e$ defined, as above (17), as the time-derivative of $\boldsymbol{b}_e$ maintaining $\boldsymbol{F}$ constant, we can write the plastic strain rate as (see also Eq. 7.18 in [17] for a particular case):

$$\boldsymbol{d}_\mathrm{p} = -\frac{1}{4}\overset{\star}{\boldsymbol{b}}_e\boldsymbol{b}_e^{-1} - \frac{1}{4}\boldsymbol{b}_e^{-1}\overset{\star}{\boldsymbol{b}}_e \tag{19}$$

from which $\boldsymbol{d}_e$ is defined as:

$$\boldsymbol{d}_e = \frac{1}{4}\dot{\boldsymbol{b}}_e\boldsymbol{b}_e^{-1} + \frac{1}{4}\boldsymbol{b}_e^{-1}\dot{\boldsymbol{b}}_e \tag{20}$$

This spatial plastic strain rate can also be obtained from the principle of maximum plastic dissipation. A more general (not restricted to elastic isotropy) of (19) for $\boldsymbol{d}_p$ was used recently by Areias and Rabczuk [7] and Areias and Matous [5] and follows similar derivations by Nemat-Nasser[6] in [50]. Note that in that case, the standard plastic strain rate $\overline{\boldsymbol{d}}_p$ in the

[5] This deduction was an essential ingredient that allowed the writing of [56].

[6] Not implemented in practice before.

intermediate configuration is used (see [7]). This particular form (19) has not, to the authors' knowledge, been used in the literature. The Voigt form of (19) allows the isolation of $\overset{\star}{\boldsymbol{b}}_e$[7]:

$$4\boldsymbol{d}_{pV} = -\boldsymbol{A}_V \overset{\star}{\boldsymbol{b}}_{eV} \tag{21}$$

where $\boldsymbol{A}_V$ is a matrix formed the components of $\boldsymbol{b}_e^{-1}$. In 3D (with 6 strain components), matrix $\boldsymbol{A}_V$ is given by:

$$\boldsymbol{A}_V = \begin{bmatrix} 2b_{e11}^{-1} & 0 & 0 & 2b_{e12}^{-1} & 2b_{e13}^{-1} & 0 \\ 0 & 2b_{e22}^{-1} & 0 & 2b_{e12}^{-1} & 0 & 2b_{e23}^{-1} \\ 0 & 0 & 2b_{e33}^{-1} & 0 & 2b_{e13}^{-1} & 2b_{e23}^{-1} \\ b_{e12}^{-1} & b_{e12}^{-1} & 0 & b_{e11}^{-1}+b_{e22}^{-1} & b_{e23}^{-1} & b_{e13}^{-1} \\ b_{e13}^{-1} & 0 & b_{e13}^{-1} & b_{e23}^{-1} & b_{e11}^{-1}+b_{e33}^{-1} & b_{e12}^{-1} \\ 0 & b_{e23}^{-1} & b_{e23}^{-1} & b_{e13}^{-1} & b_{e12}^{-1} & b_{e22}^{-1}+b_{e33}^{-1} \end{bmatrix} \tag{22}$$

with b_{eij}^{-1} being the ith row, jth column of $\boldsymbol{b}_e^{-1}$. Note that $\boldsymbol{A}_V$ is i) sparse and ii) only 6 distinct values are present. This facilitates the task of Acegen (cf. [39]) to generate very efficient code for $\boldsymbol{A}_V^{-1}$ without the full cost of a dense 6×6 inverse. In addition, complementarity (9–11) is equivalent to:

$$\mu\dot{\gamma}_i - \langle \mu\dot{\gamma}_i + \phi_i \rangle = 0 \tag{23}$$

where $\mu > 0$ is here a constant used for dimensional consistency only. Macaulay brackets $\langle \bullet \rangle \equiv \max(0, \bullet)$ are used to replace the inequalities. Note that, if (23) holds, only one of two cases occur *for each yield surface* which are independent of the value of $\mu > 0$:

- $\forall \mu > 0, \quad \mu\dot{\gamma}_i + \phi_i \geq 0 \wedge \mu\dot{\gamma}_i - \langle \mu\dot{\gamma}_i + \phi_i \rangle = 0, \Rightarrow \phi_i = 0 \Rightarrow \dot{\gamma}_i \geq 0$
- $\forall \mu > 0, \quad \mu\dot{\gamma}_i + \phi_i < 0 \wedge \mu\dot{\gamma}_i - \langle \mu\dot{\gamma}_i + \phi_i \rangle = 0, \Rightarrow \dot{\gamma}_i = 0 \Rightarrow \phi_i < 0$

In summary, the relevant constitutive equations are[8]:

$$\overset{\star}{\boldsymbol{b}}_{eV} = -4 \sum_{i=1}^{n_s} \dot{\gamma}_i \boldsymbol{A}_V^{-1} \boldsymbol{n}_{Vi} \tag{24}$$

$$\dot{\boldsymbol{v}} = -\sum_{i=1}^{n_s} \dot{\gamma}_i \boldsymbol{\varphi}_i \tag{25}$$

$$\boldsymbol{\tau}_V = 2 \left(\frac{\mathrm{d}\psi_b}{\mathrm{d}\boldsymbol{b}_e} \boldsymbol{b}_e \right)_V \tag{26}$$

$$\mu\dot{\gamma}_i - \langle \mu\dot{\gamma}_i + \phi_i \rangle = 0 \tag{27}$$

[7] The subscript V is adopted when using Voigt notation.

[8] Note that, in this context, no explicit use of the principle of maximum dissipation is required.

where $\boldsymbol{\tau}_V$ is the Kirchhoff stress in Voigt form and the V operator in (26) transforms the components of a symmetric tensor to the Voigt form. The first and last equations of this system will be subject to a specific treatment. A semi-implicit method will be used to integrate (24) and the Chen-Mangasarian smoothing procedure [23] will be applied to the non-smooth Eq. 27. The complementarity conditions are often called Karush–Kuhn– Tucker conditions (cf. [44]). Note that, in the literature, even if multiple surfaces are considered, some variant of the active-set strategy is invariably adopted (e.g. [42]). The notions of subdifferential and normal cone are classical for non-differentiable yield functions (cf. [32]) and in the convex case these can be exactly replaced by multiple yield functions.

2.2 Time integration and complementarity smoothing

The particular form of numerical solution of the constitutive system (24–27) depends on the quantity driving the flow rule. In classical discretization methods (either with mesh, such as the finite element method or meshless, such as element-free Galerkin) of finite strain problems, displacement is typically in the set of nodal degrees-of-freedom. This favors the so-called "strain-driven" methodology to constitutive integration. However, some stress components can also be prescribed, and this situation will be addressed in Sect. 2.6 (see also [38] for a small strain analysis). Two additional subscripts are used to identify the time-step. At a given time-step n indicates the previously converged value of a given quantity and $n+1$ the predicted value of the same quantity. The elastic left Cauchy-Green tensor is written at time-step $n+1$ by specializing its definition:

$$\boldsymbol{b}_{e_{n+1}} = \boldsymbol{F}_{n+1} \boldsymbol{C}_{p_n}^{-1} \boldsymbol{F}_{n+1}^T + \Delta_\star \boldsymbol{b}_e \tag{28}$$

$$= \Delta\boldsymbol{F} \boldsymbol{b}_{e_n} \Delta\boldsymbol{F}^T + \Delta_\star \boldsymbol{b}_e \tag{29}$$

where $\Delta_\star \boldsymbol{b}_e$ is the increment of $\boldsymbol{b}_e$ caused by a change in $\boldsymbol{C}_p^{-1}$ and $\Delta\boldsymbol{F} = \boldsymbol{F}_{n+1}\boldsymbol{F}_n^{-1}$. The so-called "trial" $\boldsymbol{b}_e$ is here identified here as $\boldsymbol{b}_{eo}$:

$$\boldsymbol{b}_{e\circ} = \Delta\boldsymbol{F} \boldsymbol{b}_{e_n} \Delta\boldsymbol{F}^T \tag{30}$$

The flow rule is integrated semi-implicitly; matrix $\boldsymbol{A}$ is kept constant (i.e. *frozen*) as a function of $\boldsymbol{b}_{e_n}$ and then the flow rule reads (Voigt notation is used):

$$\boldsymbol{0} = \boldsymbol{b}_{Ve\circ} - \boldsymbol{b}_{Ve_{n+1}} - 4\boldsymbol{A}_{Vn}^{-1} \boldsymbol{n}_V \Delta\boldsymbol{\gamma} \tag{31}$$

which is a nonlinear equation, part of the constitutive system. The notation $\Delta\boldsymbol{\gamma} = \{\Delta\gamma_1, \ldots, \Delta\gamma_{n_s}\}^T$, $\boldsymbol{\phi} = \{\phi_1, \ldots, \phi_{n_s}\}^T$, $\boldsymbol{\varphi} = \{\boldsymbol{\varphi}_1, \ldots, \boldsymbol{\varphi}_{n_s}\}$ and $\boldsymbol{n}_V = \{\boldsymbol{n}_{V1}, \ldots, \boldsymbol{n}_{Vn_s}\}$ is employed. Note that if $\Delta\gamma_i = 0, \quad \text{with} \quad i = 1, \ldots, n_s$ it follows that $\boldsymbol{b}_{Ve_{n+1}} = \boldsymbol{b}_{Ve\circ}$ and Eq. 31 is trivially satisfied. Internal variable evolution is integrated with the classical backward-Euler method:

$$\mathbf{0} = \boldsymbol{v}_n - \boldsymbol{v}_{n+1} + \boldsymbol{\varphi}\Delta\boldsymbol{\gamma} \tag{32}$$

In addition to these two equations, the complementarity conditions can be written in vector form as:

$$\mu^\star\Delta\boldsymbol{\gamma} - \langle\mu^\star\Delta\boldsymbol{\gamma} + \boldsymbol{\phi}\rangle = \mathbf{0} \tag{33}$$

with $\Delta\boldsymbol{\gamma} = \{\Delta\gamma_1, \ldots, \Delta\gamma_{n_s}\}^T$ and $\boldsymbol{\phi} = \{\phi_1, \ldots, \phi_{n_s}\}^T$. We then have the following set of constitutive unknowns:

$$\boldsymbol{\chi} = \{\boldsymbol{b}_{Ve_{n+1}}, \Delta\boldsymbol{\gamma}, \boldsymbol{v}_{n+1}\}^T \tag{34}$$

and, as a nonlinear system,

$$\boldsymbol{e} = \{(31), (33), (32)\}^T \tag{35}$$

Since we did not use the exponential integrator (see, e.g. [58] for a discussion), incompressibility is not exactly satisfied. However, it can be enforced as an additional equation. Equation 33 can also be written as:

$$\boldsymbol{\phi}^\star(\Delta\boldsymbol{\gamma}, \boldsymbol{b}_{Ve_{n+1}}, \boldsymbol{v}_{n+1}) = \mu^\star\Delta\boldsymbol{\gamma} - \langle\mu^\star\Delta\boldsymbol{\gamma} + \boldsymbol{\phi}\rangle = \mathbf{0} \tag{36}$$

At the Gauss point level, Newton's method of solution is used to determine (34) from (35). Therefore, the derivative of the system with respect to the constitutive unknowns is required. For conciseness, we introduce the following notation[9]:

$$\boldsymbol{m} = \boldsymbol{A}_{Vn}^{-1}\boldsymbol{n}_V \tag{37}$$

$$[\boldsymbol{M}]_{ijk} = \frac{\partial[\boldsymbol{m}]_{ij}}{\partial[\boldsymbol{b}_{Ve}]_k} = \frac{\partial[\boldsymbol{m}]_{ij}}{\partial[\boldsymbol{\tau}_V]_l}\frac{\partial[\boldsymbol{\tau}_V]_l}{\partial[\boldsymbol{b}_{Ve}]_k} = \left[\boldsymbol{A}_{Vn}^{-1}\right]_{in}\frac{\partial[\boldsymbol{n}_V]_{nj}}{\partial[\boldsymbol{\tau}_V]_l}\frac{\partial[\boldsymbol{\tau}_V]_l}{\partial[\boldsymbol{b}_{Ve}]_k} \tag{38}$$

$$[\boldsymbol{N}]_{ijk} = \frac{\partial[\boldsymbol{m}]_{ij}}{\partial[\boldsymbol{v}_{n+1}]_k} \tag{39}$$

$$[\nabla\boldsymbol{\phi}^\star]^b_{ij} = \frac{\partial[\boldsymbol{\phi}^\star]_i}{\partial[\boldsymbol{\tau}_V]_k}\frac{\partial[\boldsymbol{\tau}_V]_k}{\partial[\boldsymbol{b}_{Ve}]_j} \tag{40}$$

$$[\nabla\boldsymbol{\phi}^\star]^\gamma_{ij} = \frac{\partial[\boldsymbol{\phi}^\star]_i}{\partial[\boldsymbol{\gamma}]_j} \tag{41}$$

$$[\nabla\boldsymbol{\phi}^\star]^v_{ij} = \frac{\partial[\boldsymbol{\phi}^\star]_i}{\partial[\boldsymbol{v}]_j} \tag{42}$$

$$[\nabla\boldsymbol{\varphi}]^b_{ijk} = \frac{\partial[\boldsymbol{\varphi}]_{ij}}{\partial[\boldsymbol{b}_{Ve}]_k} \tag{43}$$

$$[\nabla\boldsymbol{\varphi}]^\gamma_{ijk} = \frac{\partial[\boldsymbol{\varphi}]_{ij}}{\partial[\boldsymbol{\gamma}]_k} \tag{44}$$

[9] Note that $\boldsymbol{A}_n$ is constant, which significantly simplifies the calculations.

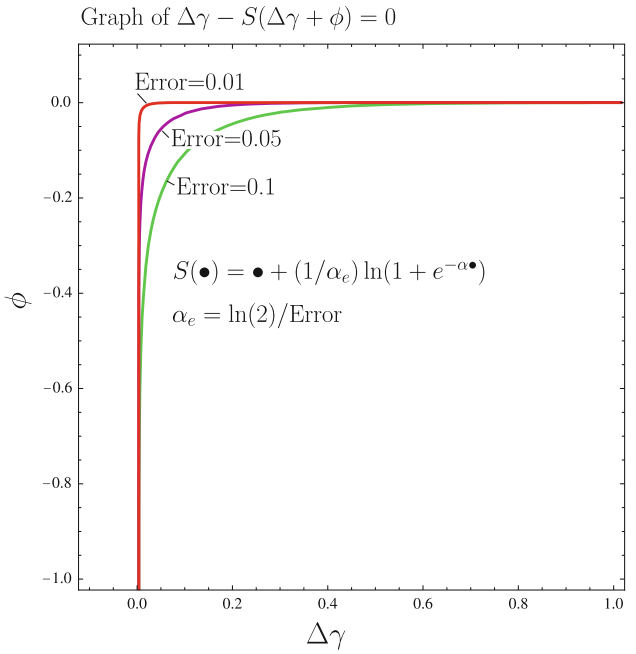

Fig. 1 Replacement of $\mu^\star\Delta\gamma_i - \langle\mu^\star\Delta\gamma_i + \phi_i\rangle$ by $\mu^\star\Delta\gamma_i - S(\mu^\star\Delta\gamma_i + \phi_i)$ as a function of a Error parameter ($\mu^\star = 1$ is depicted)

$$[\nabla\boldsymbol{\varphi}]^v_{ijk} = \frac{\partial[\boldsymbol{\varphi}]_{ij}}{\partial[\boldsymbol{v}]_k} \tag{45}$$

It is noticeable that nested derivatives emerge due to interdependence:

$$\boldsymbol{J} = \frac{\partial\boldsymbol{e}}{\partial\boldsymbol{\chi}} = \begin{bmatrix} -\delta_{ij} - 4[\boldsymbol{M}]_{ikj}[\Delta\boldsymbol{\gamma}]_k & -4[\boldsymbol{m}]_{ij} & -4[\boldsymbol{N}]_{ikj}[\Delta\boldsymbol{\gamma}]_k \\ [\nabla\boldsymbol{\phi}^\star]^b_{ij} & [\nabla\boldsymbol{\phi}^\star]^\gamma_{ij} & [\nabla\boldsymbol{\phi}^\star]^v_{ij} \\ [\nabla\boldsymbol{\varphi}]^b_{ikj}[\Delta\boldsymbol{\gamma}]_k & [\boldsymbol{\varphi}]_{ij} + [\nabla\boldsymbol{\varphi}]^\gamma_{ikj}[\Delta\boldsymbol{\gamma}]_k & -\delta_{ij} + [\nabla\boldsymbol{\varphi}]^v_{ikj}[\Delta\boldsymbol{\gamma}]_k \end{bmatrix} \tag{46}$$

In addition to this Jacobian, $\boldsymbol{e}$ also depends on $\boldsymbol{b}_{Ve\circ}$. The derivative of $\boldsymbol{e}$ with respect to $\boldsymbol{b}_{e\circ}$ is given by:

$$\boldsymbol{L} = \frac{\partial\boldsymbol{e}}{\partial\boldsymbol{b}_{Ve\circ}} = \begin{bmatrix} -4[\boldsymbol{M}]_{ikj}[\Delta\boldsymbol{\gamma}]_k \\ [\nabla\boldsymbol{\phi}^\star]^b_{ij} \\ [\nabla\boldsymbol{\varphi}]^b_{ikj}[\Delta\boldsymbol{\gamma}]_k \end{bmatrix} \tag{47}$$

The relations (33) are replaced by the smooth ramp function of Chen and Mangasarian [24]. Consequences of this replacement were discussed by Areias and Rabczuk [7]. Figure 1 shows the effect of this replacement in the satisfaction of the complementarity condition.

One can observe that, the classical effective plastic strain $\varepsilon_{p_{n+1}}$ is not typically included in $[\nabla\boldsymbol{\phi}^\star]^v_{ij}$. The reason for

this is that $\varepsilon_{p_{n+1}}$ can be related to the remaining iterative quantities. Using the backward-Euler method, $\varepsilon_{p_{n+1}}$ reads[10]

$$\varepsilon_{p_{n+1}} = \varepsilon_{p_n} + \sqrt{\frac{2}{3}}\,\|\boldsymbol{n}_V \Delta\boldsymbol{\gamma}\|_V \tag{48}$$

where $\|\bullet\|_V$ is the Voigt norm of a tensor $\bullet$ or the Frobenius norm of the corresponding matrix. The variation of (48) can be written in the following format:

$$\begin{aligned}\mathrm{d}\varepsilon_{p_{n+1}} &= \sqrt{\frac{2}{3}}\frac{\mathrm{d}\|\boldsymbol{n}_V \Delta\boldsymbol{\gamma}\|_V}{\mathrm{d}\left[\boldsymbol{n}_V \Delta\boldsymbol{\gamma}\right]_m} \\ &\times \left(\frac{\partial\left[\boldsymbol{n}_V\right]_{mp}}{\partial\left[\boldsymbol{\tau}_V\right]_l}\frac{\partial\left[\boldsymbol{\tau}_V\right]_l}{\partial\left[\boldsymbol{b}_{Ve}\right]_k}\left[\Delta\gamma\right]_p \mathrm{d}\left[\boldsymbol{b}_{Ve}\right]_k + \left[\boldsymbol{n}_V\right]_{mp}\left[\mathrm{d}\Delta\gamma\right]_p\right)\end{aligned} \tag{49}$$

This relation is rarely shown (we couldn't find it in the literature) and, of course it is crucial to ensure the quadratic rate of convergence. Equation 48 is generally used despite being appropriate for the von-Mises yield surface. For general yield criteria, we consider two cases: a multi-surface yield criterion with a single hardening variable ε_p or each surface equipped with hardening variables ε_p^i with $i = 1, \ldots, n_s$. Equivalence of plastic dissipation provides the rationale for determining the effective plastic strain:

$$\sigma_{eq_i}\dot{\varepsilon}_p^i = \dot{\gamma}_i \boldsymbol{n}_i : \boldsymbol{\tau}, \quad i = 1, \ldots, n_s \tag{50}$$

In the first case, an approach would consist in summing each term $i = 1, \ldots, n_s$ in (50):

$$\varepsilon_{p_{n+1}} = \varepsilon_{p_n} + \sum_{i=1}^{n_s} \Delta\gamma_i \frac{\boldsymbol{n}_i : \boldsymbol{\tau}}{\sigma_{\mathrm{eq}_i}} \tag{51}$$

In the second case, each surface is associated to a given hardening variable ε_p^i with $i = 1, \ldots, n_s$:

$$\varepsilon_{p_{n+1}}^i = \varepsilon_{p_n}^i + \Delta\gamma_i \frac{\boldsymbol{n}_i : \boldsymbol{\tau}}{\sigma_{eq_i}} \tag{52}$$

For both cases, the variation of $\varepsilon_{p_{n+1}}^i$ is required for the use of Newton's method of solution:

$$\begin{aligned}\mathrm{d}\varepsilon_{p_{n+1}}^i &= \frac{\boldsymbol{n}_i : \boldsymbol{\tau}}{\sigma_{eq_i}}\mathrm{d}\Delta\gamma_i \\ &+ \left[\frac{\Delta\gamma_i}{\sigma_{eq_i}}\left(\boldsymbol{\tau} : \frac{\mathrm{d}\boldsymbol{n}_i}{\mathrm{d}\boldsymbol{\tau}} + \boldsymbol{n}_i\right) - \frac{\boldsymbol{n}_i : \boldsymbol{\tau}}{\sigma_{eq}}\right] : \frac{\partial\boldsymbol{\tau}}{\partial\boldsymbol{b}_e} : \mathrm{d}\boldsymbol{b}_e\end{aligned} \tag{53}$$

note that in this derivation (53) double contractions are actually performed using the Voigt form by doubling the shear components contribution.

For independent yield criteria, clearly (51) would be preferably employed. However, for classical multi-surface yield criteria, (52) would be more appropriate. The reader can observe that our present approach departs from classical $\boldsymbol{F}_e\boldsymbol{F}_p$ "principal directions" algorithmia [20,58] but also from extensions to small strain classical derivations (see, e.g. [34, 46]). No return-mapping is necessary and all yield criteria can be included without modifications to the framework.

[10] This form follows directly from the general expression in the seminal work of Lubliner [44] and can be specialized for each yield criterion.

2.3 Constant flow vectors

Certain yield criteria have constant flow vectors in the sense that dependence may occur with respect to $\boldsymbol{F}$ but not with respect to $\boldsymbol{b}_e$ and $\boldsymbol{v}_{n+1}$. This is the case of classical Schmid single-crystal plasticity and of many models of J_2 plasticity (cf. [48,54]). In addition, functions $\boldsymbol{\varphi}$ can be related with $\boldsymbol{v}_{n+1}$ in a simpler form than previously shown, and therefore iteration in $\Delta\boldsymbol{\gamma}_i$ only is possible. Advantage is taken of this fact to further simplify the algorithm and the linearization. The plastic multipliers can be determined by a reduced Newton iteration:

$$\left(\left[\nabla\boldsymbol{\phi}^\star\right]_{ij}^{\gamma} - 4\left[\nabla\boldsymbol{\phi}^\star\right]_{ik}^{b}\left[\boldsymbol{m}\right]_{kj}\right)\mathrm{d}\Delta\gamma_j + \left[\nabla\boldsymbol{\phi}\right]_{ij}^{v}\mathrm{d}v_j = -\phi_i \tag{54}$$

$$\begin{aligned}\mathrm{d}v_k = &\left(\left[\boldsymbol{I}\right]_{jk} - \left[\nabla\boldsymbol{\varphi}\right]_{jik}^{v}\Delta\gamma_i\right)^{-1} \\ &\times\left(\left[\nabla\boldsymbol{\varphi}\right]_{jil}^{\gamma}\Delta\gamma_i + \left[\boldsymbol{\varphi}\right]_{jl} - 4\left[\nabla\boldsymbol{\varphi}\right]_{jin}^{b}\left[\boldsymbol{m}\right]_{ln}\Delta\gamma_i\right)\mathrm{d}\Delta\gamma_l\end{aligned} \tag{55}$$

where (55) will be replaced in (54) to write a Newton iteration in $\Delta\boldsymbol{\gamma}$. This iteration may be of more difficult solution than a combined iteration in $\Delta\boldsymbol{\gamma}$ and $\boldsymbol{v}$ which will have more unknowns but typically a larger radius of convergence.

2.4 Explicit inversion of an affine relation between $\boldsymbol{b}_{Ve}$ and $\boldsymbol{\tau}_V$ (metal plasticity)

In the case where it is possible to explicitly invert the relation between $\boldsymbol{b}_{Ve}$ and $\boldsymbol{\tau}_V$, multiplications in (38), (39) can be avoided, which results in considerable computational savings since matrix-matrix multiplications are $\bigcirc(n_V^3)$ operations, with n_V being the number of Voigt components. Specifically, we can iterate for $\boldsymbol{\tau}_V$ directly (as in small strain elasto-plasticity, cf. [44,60]). The quasi-incompressible Neo-Hookean elasticity law can be further simplified, even without the traditional deviatoric/volumetric split. The latter was explored in very particular conditions (J_2 plasticity) in Ref. [57] with the dilatational part of the flow vector ($\boldsymbol{n}$) being null. If small elastic strains are considered, this would result in a very efficient alternative to the hypoelastic procedures (cf. [34]). Interestingly, a plastic predictor can also be used (see also [50]). If an affine relation between $\boldsymbol{\tau}_V$ and $\boldsymbol{b}_{Ve}$ is employed the following law is possible:

$$\boldsymbol{\tau}_V = \boldsymbol{C}_{\mathrm{linear}}\left(\boldsymbol{b}_{Ve} - \boldsymbol{I}_2\right) \tag{56}$$

Table 1 Tested yield criteria

Yield criterion	Number of yield surfaces	Equivalent stresses
von-Mises	1	$\sigma_{\mathrm{eq}_1} = \sqrt{I_1^2 - 3I_2}$
Tresca	6	$\sigma_{\mathrm{eq}_k} = \widetilde{\tau}_i - \widetilde{\tau}_j, \quad i \neq j$
Ductile damage	2	$\sigma_{eq_1} = \frac{\sqrt{I_1^2 - 3I_2} - f c_1 I_1}{1-f}$
		$\sigma_{eq_2} = \frac{\sqrt{I_1^2 - 3I_2}}{1-f}$
Plane Hill criterion ($\boldsymbol{\tau}' = \boldsymbol{T}^T \boldsymbol{\tau} \boldsymbol{T}$)	1	$\sigma_{\mathrm{eq}_1} = \sqrt{f_H(\tau'_{22} - \tau'_{33})^2 + g_H(\tau'_{33} - \tau'_{11})^2 + h_H(\tau'_{11} - \tau'_{22})^2 + 2n_H \tau'^2_{12}}$
$I_1 = \mathrm{tr}\boldsymbol{\tau}$, $I_2 = \frac{1}{2}\left[(\mathrm{tr}\boldsymbol{\tau})^2 - \mathrm{tr}\boldsymbol{\tau}^2\right]$, $I_3 = \det \boldsymbol{\tau}$		
$\boldsymbol{T} = \{\{\cos(\theta), -\sin(\theta)\}, \{\sin(\theta), \cos(\theta)\}\}$		$f_H = \frac{1}{2}(1 - r_{1c} + r_{2c})$
		$g_H = \frac{1}{2}(1 + r_{1c} - r_{2c})$
		$h_H = \frac{1}{2}(r_{1c} + r_{2c} - 1)$
		$n_H = \frac{1}{2} r_{12c}$

Table 2 Tested hyperelastic strain energy densities

Hyperelastic law	Kirchhoff stress
Neo-Hookean (quasi-incompressible)	$\boldsymbol{\tau} = G\,(\det \boldsymbol{b}_e)^{-\frac{1}{3}} \left(\boldsymbol{b}_e - \frac{1}{3}\mathrm{tr}\left[\boldsymbol{b}_e\right]\boldsymbol{I}\right) + \kappa\sqrt{\det \boldsymbol{b}_e}\left(\sqrt{\det \boldsymbol{b}_e} - 1\right)\boldsymbol{I}$
Metal plasticity	$\boldsymbol{\tau} = \frac{\mathrm{d}\boldsymbol{\tau}}{\mathrm{d}\boldsymbol{b}_e}\vert_{\boldsymbol{b}_e = \boldsymbol{I}}\,(\boldsymbol{b}_e - \boldsymbol{I})$

where Voigt form is used with $\boldsymbol{I}_2 = \{1, 1, 1, 0, 0, 0\}^T$ for $n_V = 6$. With (56) the following system arises:

$$\boldsymbol{C}^{-1}_{\mathrm{linear}} \Delta\boldsymbol{\tau}_V - 4\boldsymbol{A}_n^{-1}\boldsymbol{n}_V \Delta\boldsymbol{\gamma} = \boldsymbol{0} \tag{57}$$

$$\boldsymbol{v}_n - \boldsymbol{v}_{n+1} + \boldsymbol{\varphi}\Delta\boldsymbol{\gamma} = \boldsymbol{0} \tag{58}$$

$$\mu^\star \Delta\boldsymbol{\gamma} - \left\langle \mu^\star \Delta\boldsymbol{\gamma} + \boldsymbol{\phi} \right\rangle = 0 \tag{59}$$

with $\boldsymbol{\tau}_V = \boldsymbol{\tau}_{e0} + \Delta\boldsymbol{\tau}$. Constitutive unknowns are now $\Delta\boldsymbol{\tau}_V$, $\Delta\boldsymbol{\gamma}$ and $\boldsymbol{v}_{n+1}$. The same procedure as before is adopted to calculate the tangent modulus. For metal plasticity, this seems appropriate since $\boldsymbol{b}_e$ is close enough to the unit ($\boldsymbol{b}_e = \boldsymbol{I}$) and has many advantages with respect to the classical objective-rate approaches. Perhaps the most useful being the number of operations to determine the consistent tangent modulus.

2.5 Linearization

The constitutive spatial modulus is required to use in the element tangent stiffness matrix, which in turn is used in the Multilevel-Newton's algorithm (please consult the inaugural work of Hartmann [30] concerning this important topic). Newton's method of solution is applied at two levels: the Gauss point level and the equilibrium level. With that goal, the total derivative of $\boldsymbol{\tau}_{n+1}$ with respect to $\boldsymbol{F}_{n+1}$ (4) is given by the chain rule of derivation:

$$\frac{\mathrm{d}\boldsymbol{\tau}_{Vn+1}}{\mathrm{d}\boldsymbol{F}_{n+1}} = \frac{\partial \boldsymbol{\tau}_{Vn+1}}{\partial \boldsymbol{b}_{Ve\circ}} \left(\boldsymbol{I}_4 - \boldsymbol{T}_{e\circ}\right) \frac{\partial \boldsymbol{b}_{Ve\circ}}{\partial \boldsymbol{F}_{n+1}} \tag{60}$$

where the constitutive-independent derivative is given by:

$$\frac{\partial \left[\boldsymbol{b}_{e\circ}\right]_{ij}}{\partial \left[\boldsymbol{F}_{n+1}\right]_{mn}} = \left[\boldsymbol{I}\right]_{im}\left[\boldsymbol{F}_{n+1}\right]_{jl}\left[\widetilde{\boldsymbol{b}}\right]_{nl} + \left[\boldsymbol{F}_{n+1}\right]_{ik}\left[\boldsymbol{I}_{n+1}\right]_{jm}\left[\widetilde{\boldsymbol{b}}\right]_{kn} \tag{61}$$

and $\widetilde{\boldsymbol{b}} = \boldsymbol{F}_n^{-1}\boldsymbol{b}_n\boldsymbol{F}_n^{-T}$. Matrix $\boldsymbol{T}_{e\circ}$ in (60) is determined by the product:

$$\boldsymbol{T}_{e\circ} = \boldsymbol{T}_{\boldsymbol{b}}\boldsymbol{J}^{-1}\boldsymbol{L} \tag{62}$$

with $\boldsymbol{T}_{\boldsymbol{b}}$ being a matrix which filters all rows of $\boldsymbol{J}^{-1}$ not related with the derivative with respect to $\boldsymbol{b}$. Finally, the derivative of $\boldsymbol{\tau}_V$ with respect to $\boldsymbol{b}_{Ve\circ}$ is determined analytically by Mathematica with the Acegen add-on [39]. For the simplified case (Sect. 2.3) the linearization can also directly obtained and is therefore omitted. We remark that the tangent matrix (4) is not major-symmetric as in classical works and a non-symmetric linear sparse solver is *required*.

2.6 Mixed control

In addition to the purely constitutive equations, it often occurs that some component (or components) of stress has a known value (plates, shells and beams are classical examples where known values of stress exist), independent of the constitutive models. Of course, this subject has been dealt in the context of anisotropic elasticity and finite strain *isotropic* plasticity [37] but not in the most general case. For small strains, the work of Klisinski [38] (who coined the term *mixed control*)

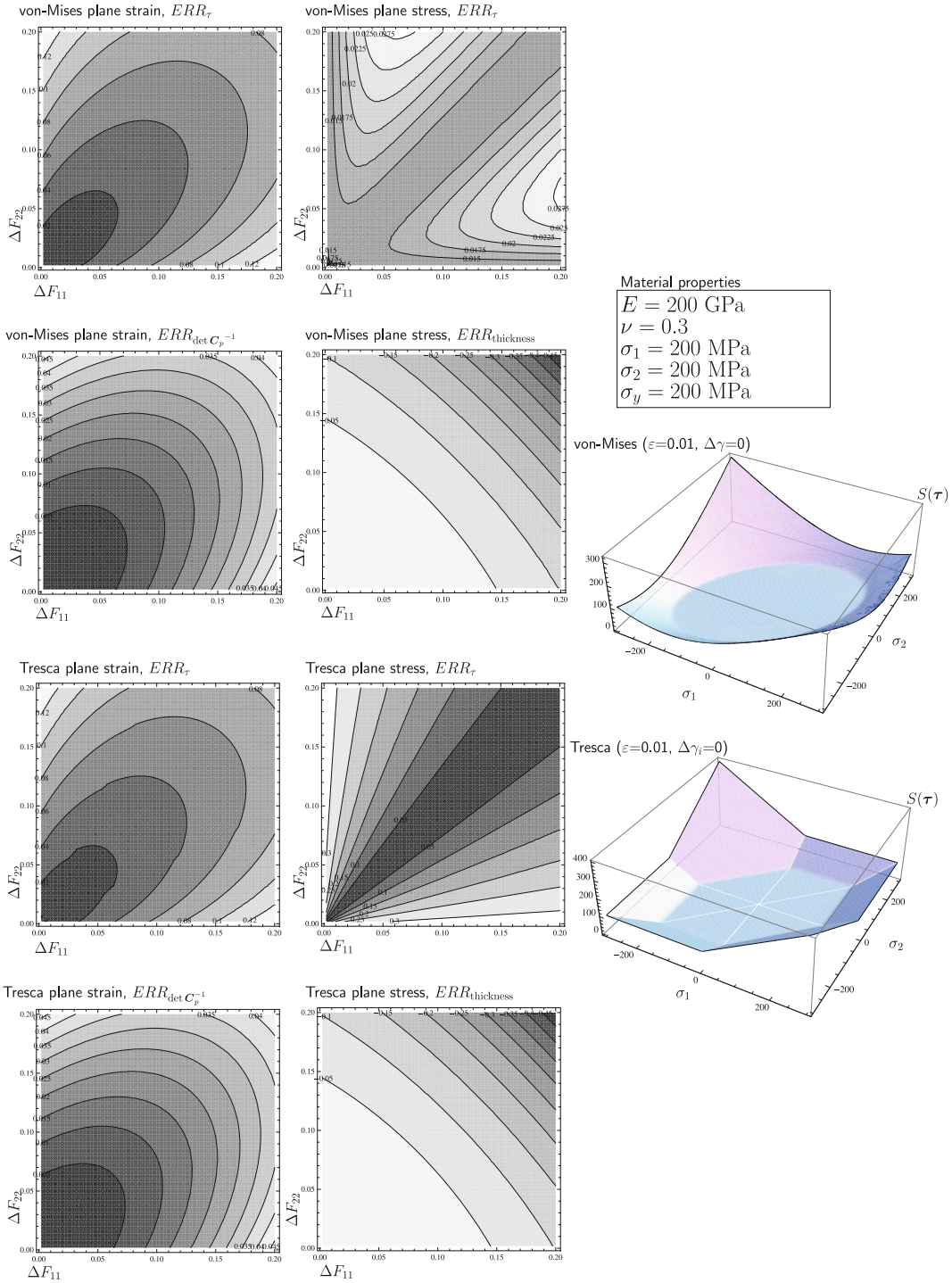

Fig. 2 Isoerror maps and representation of two classical yield criteria (current implementation)

shows that stress and strain components can be used as control variables and a uniqueness condition was derived. Finite strains introduce some further calculations, as we shall see. We use a transformation method to provide a general solution to this problem. In its simplest form, a m-dimensional function of $\boldsymbol{F}$, $\boldsymbol{f}(\boldsymbol{F})$, is enforced:

$$\boldsymbol{f}(\boldsymbol{F}) = \boldsymbol{0} \tag{63}$$

The image of function $\boldsymbol{f}(\boldsymbol{F})$ can be, for example, a stress component. We partition the components of $\boldsymbol{F}$ in retained (r) $\boldsymbol{F}_r$ and slave (s) $\boldsymbol{F}_s$ parts: $\boldsymbol{F} = \boldsymbol{F}_r + \boldsymbol{F}_s$[11] where the number of independent components of $\boldsymbol{F}_s$ is m. The derivative of τ_{ij} with respect to F_{kl} is obviously used in Newton method

[11] Typically, F_{33} is the slave part of the deformation gradient in a shell, when covariant coordinates are used.

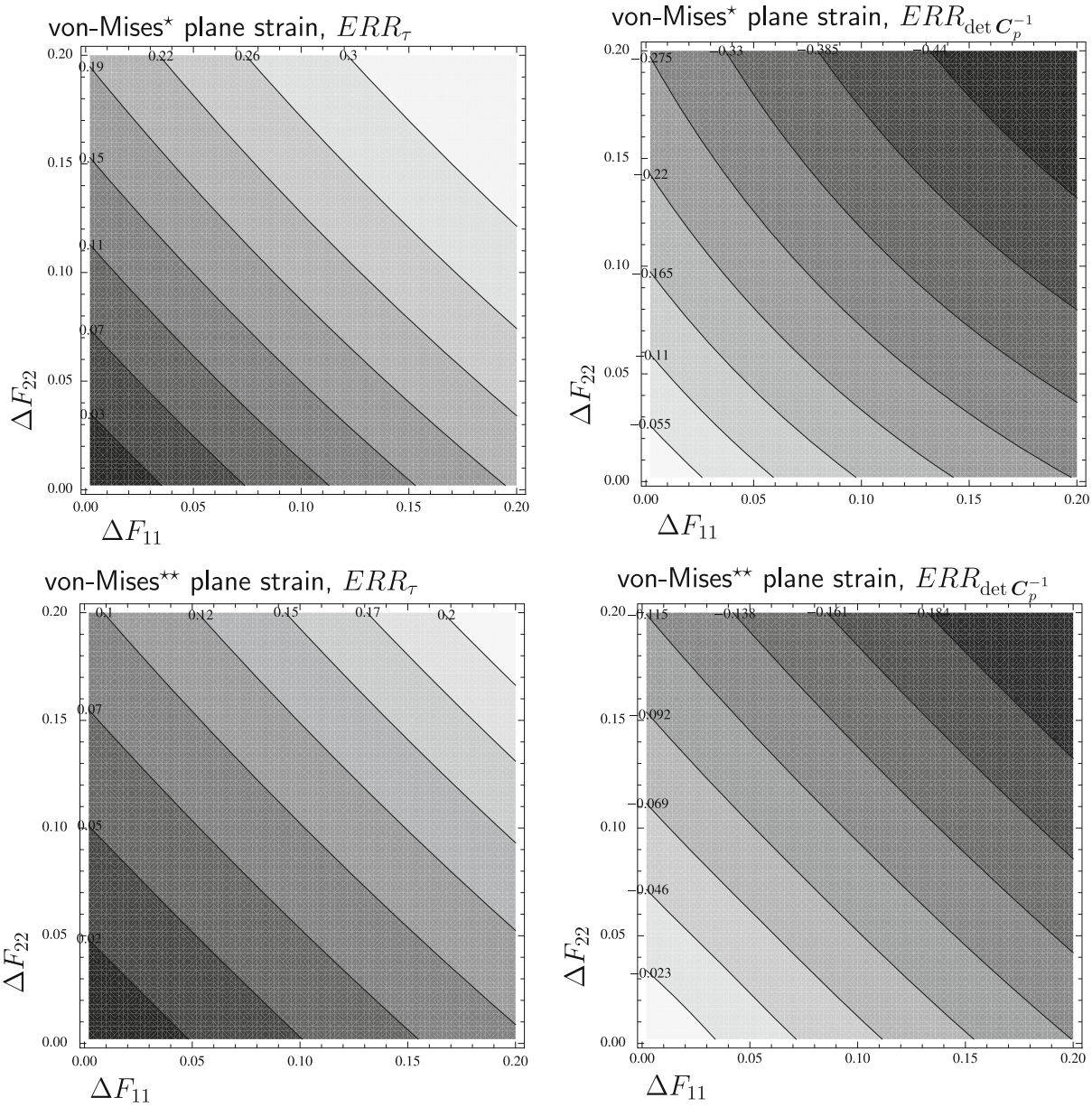

Fig. 3 Iso-error maps of two classical finite-strain plasticity models: Simo 1988 [56,57] (⋆) and Simo 1992 [58] (⋆⋆) models

to enforce (63). This condition is enforced outside the constitutive iteration since it adds further non-linearities which reduce the convergence radius.

Linearization of $\boldsymbol{f}(\boldsymbol{F})$ and non-singularity of $\partial \boldsymbol{f}/\partial \boldsymbol{F}_s$ reads

$$\mathrm{d}\boldsymbol{F}_s = -\left(\frac{\partial \boldsymbol{f}}{\partial \boldsymbol{F}_s}\right)^{-1} \boldsymbol{f} - \left(\frac{\partial \boldsymbol{f}}{\partial \boldsymbol{F}_s}\right)^{-1} \frac{\partial \boldsymbol{f}}{\partial \boldsymbol{F}_r} : \mathrm{d}\boldsymbol{F}_r \tag{64}$$

Then the derivative of $\boldsymbol{\tau}$ with respect to $\boldsymbol{F}_r$ which will be required for the element technology part of the implementation is obtained *after convergence* of (63) and the inner constitutive system. The variation of $\boldsymbol{\tau}$ with respect to $\boldsymbol{F}_r$ is then given by:

$$\mathrm{d}\boldsymbol{\tau} = \frac{\mathrm{d}\boldsymbol{\tau}}{\mathrm{d}\boldsymbol{F}} : \left(\boldsymbol{I} - \left(\frac{\partial \boldsymbol{f}}{\partial \boldsymbol{F}_s}\right)^{-1} \frac{\partial \boldsymbol{f}}{\partial \boldsymbol{F}_r}\right) : \mathrm{d}\boldsymbol{F}_r \tag{65}$$

Plane stress condition is applied for $m = 1$, $\boldsymbol{f} = \{\tau_{33}\}\boldsymbol{F}_s = \{F_{33}\}$. The corresponding thickness field is determined from $F_{33} : h = F_{33} H$ where H is the undeformed thickness and h is the deformed counterpart. For beams, two normal stress components are set to zero. A formal analysis of this procedure was performed recently (cf. Areias et al. [9]) and is much more complex than what is presented here. In addition, as was sharply pointed by a referee of this work, transverse shear stresses can occur in general. However, to avoid this possibility we make use of our recent model ([10]) where the

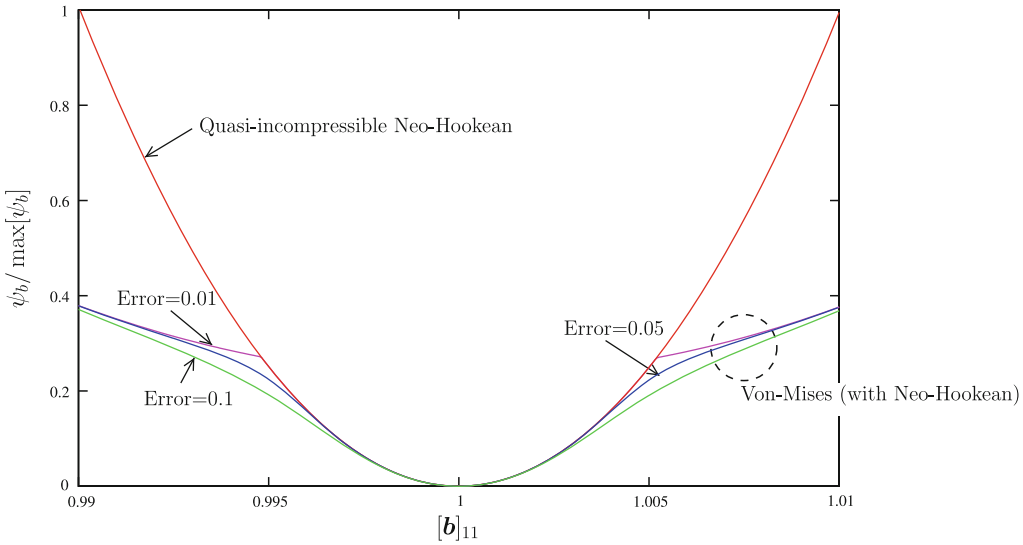

Fig. 4 Effect of Error in the strain energy density value and results for loading

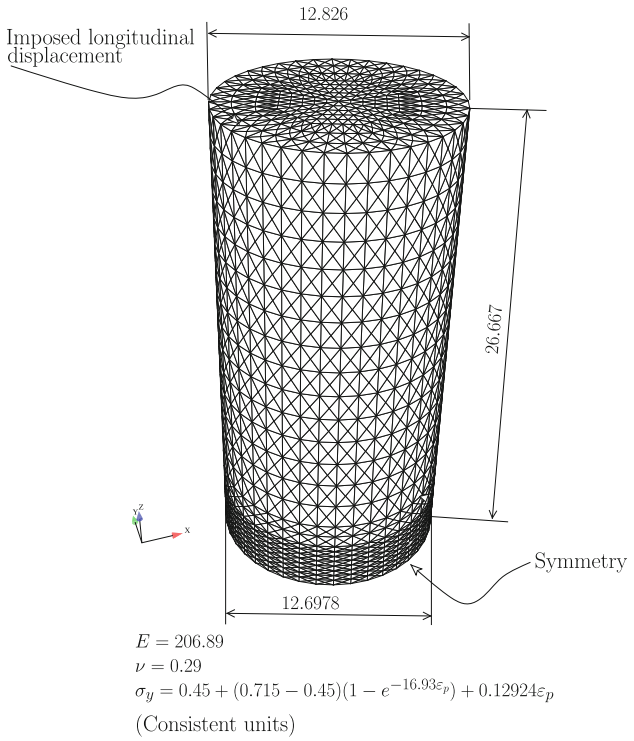

Fig. 5 Relevant dimensions and mesh for the tension test

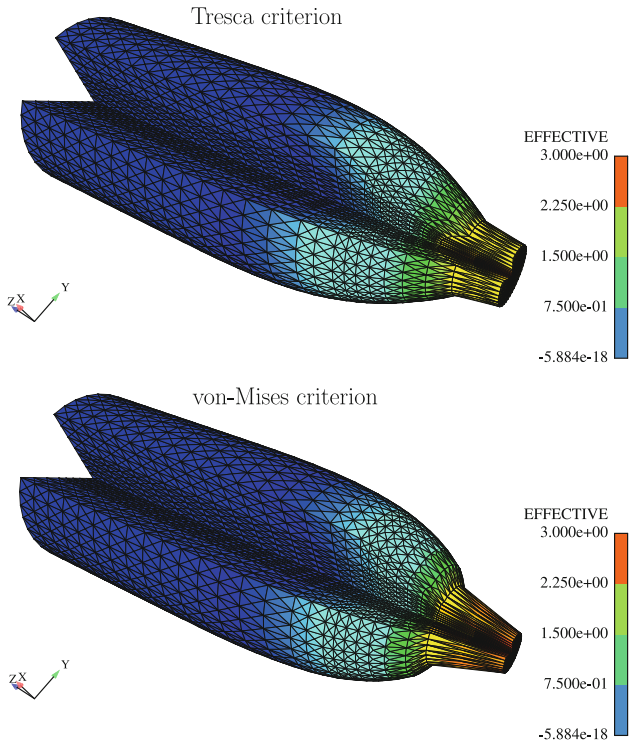

Fig. 6 Tresca and von-Mises effective plastic strain contour plot

Kirchhoff-Love hypothesis is adopted. Note that this is theoretically supported, as discussed by Antman [1] and more specifically by Antman and Marlow [2] where the consequences of the Kirchhoff-Love hypothesis were studied.

2.7 Least-square projection in trial principal directions for specific isotropic yield criteria

Since the work of Weber and Anand [63], Simo [58] and Souza Neto et al. [52], it was found convenient for isotropic flow rules which do not alter or slightly alter the elastic principal directions, to iterate in the reduced principal space. If isotropic elasticity coaxiality between $\boldsymbol{b}_e$ and $\boldsymbol{\tau}$ is satisfied and the so-called "return mapping" maintains this coaxiality,[12] then this approach is exact (this is the case of radial return[36]). Although we are interested in more general laws, it is now important to view these approaches under our

[12] It *requires* a coaxial flow rule.

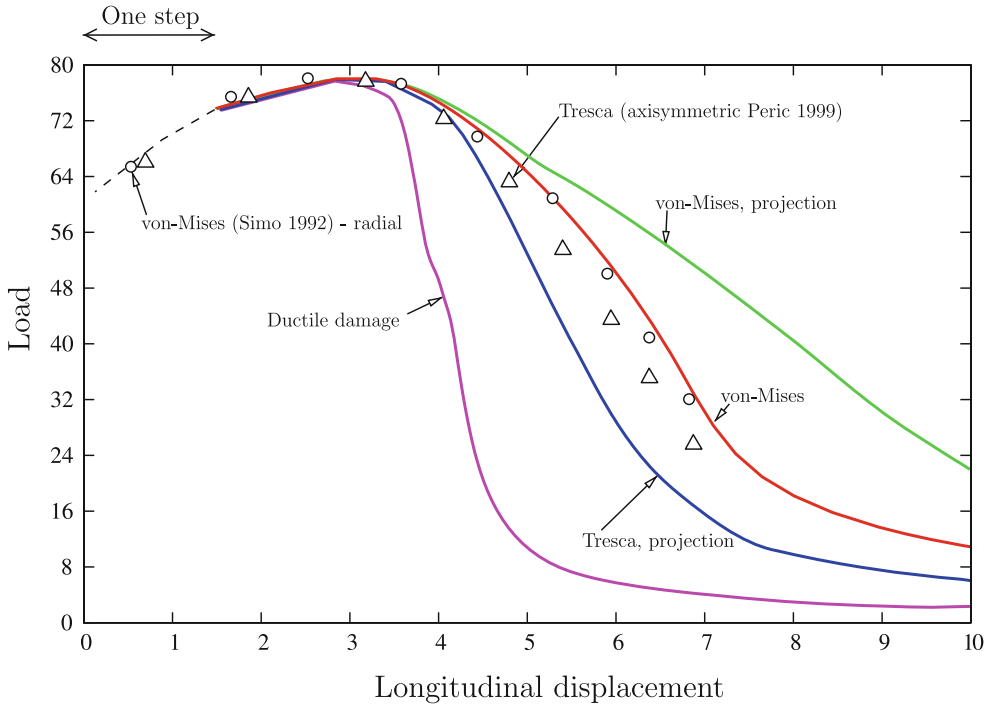

Fig. 7 Load versus longitudinal displacement results for von-Mises with and without projection and Tresca criterion. Also shown are results from Simo's work [58] and Peric and de Souza Neto's work with axisymmetric elements [52]

own method. We use a projection technique so that isotropic laws use approximate eigenvectors. The idea is to perform a decomposition of $\boldsymbol{b}_e^\star$:

$$\boldsymbol{b}_e^\star = \lambda_i^2 \boldsymbol{n}_i \otimes \boldsymbol{n}_i \tag{66}$$

where λ_i are the principal trial elastic stretches and $\boldsymbol{n}_i$ are the corresponding spatial eigenvectors. We use $\boldsymbol{E}_i = \boldsymbol{n}_i \otimes \boldsymbol{n}_i$ in Voigt format and perform a least-square projection of $\boldsymbol{\tau}$ using $\boldsymbol{E}_i$ as basis:

$$\min_{\tau_i} \frac{1}{2} (\boldsymbol{\tau} - \widetilde{\tau}_i \boldsymbol{E}_i) : (\boldsymbol{\tau} - \widetilde{\tau}_i \boldsymbol{E}_i) \tag{67}$$

which results for $\widetilde{\tau}_i$:

$$\widetilde{\tau}_i = \left[\boldsymbol{E}_i : \boldsymbol{E}_j\right]^{-1} \left\{\boldsymbol{E}_j : \boldsymbol{\tau}\right\} \tag{68}$$

and, for the derivative (in Voigt form $j = 1, \ldots, n_V$ with n_V being the number of Voigt components),

$$\frac{\partial \widetilde{\tau}_i}{\partial \tau_j} = \left[\boldsymbol{E}_i : \boldsymbol{E}_k\right]^{-1} \left[\boldsymbol{E}_k\right]_j \tag{69}$$

This procedure is exact for the flow rule proposed by Simo [58,60][13] if the von-Mises yield criterion is used, and approximate in general. For principal-stress based criteria with corners, it allows large load steps to be used since the eigenprojections $\boldsymbol{E}_i$ are kept constant during constitutive integration. This was the *leitmotiv* in [52]. Obviously, $\widetilde{\tau}_i$ depends on $\boldsymbol{b}_e^\star$, and therefore on $\boldsymbol{F}$ by means of the eigenprojections $\boldsymbol{E}_i$ which increases the linearization cost (for the analytical derivation, cf. [27]). We use Mathematica with the Acegen add-on to calculate the derivative. The well-known corner vicissitude in Tresca and Mohr-Coulomb yield criteria (sharply diagnosed by de Borst [26]) is definitely solved by using multi-surface plasticity with either the present least-square technique or the principal direction geometric method in [52]. When combined with our smoothing technique, no active-set strategy is required. Note that, if there is substantial time change in $\boldsymbol{n}_i$, then artificial locking occurs, as we will observe.

[13] Which does not coincide with the present one.

2.8 Prototype and test constitutive laws

Table 1 shows the prototype yield criteria used for the assessment and numerical examples sections. The ductile damage criterion was adopted recently to deal with differences between tension and compression for ductile materials in a simpler form than the Rousselier proposal [53] (Table 2).

2.9 Mixed finite element technology for incompressible and quasi-incompressible problems

For 3D elements based on the low-order tetrahedron technology, we employ a MINI-like (cf. Arnold [13]) element which was analyzed and used in [5–7]. The inf-sup test was performed by the first Author successfully for several well

Table 3 Tension test: constitutive properties (consistent units)

E	206.9
ν	0.29
σ_y	$0.45 + (0.715 - 0.45)(1 - e^{-16.93\varepsilon_p}) + 0.12929\varepsilon_p$
Criterion #1	von-Mises
Criterion #2	von-Mises (with projection)
Criterion #3	Tresca (with projection)
Criterion #4	Ductile damage

known benchmarks. The degrees-of-freedom are: nodal displacements at the 4 nodes of the tetrahedron and an internal bubble whose additional degrees-of-freedom are condensed out. In addition, pressure degrees-of-freedom are used in the corner nodes. The pressure field (p) is tied to the displacement field by a standard approach: the internal virtual work is given by:

$$\delta W_i = \int_{\Omega_0} \{[\mathrm{Dev}]\boldsymbol{\tau} : \nabla\delta\boldsymbol{x} + p\boldsymbol{I} : \nabla\delta\boldsymbol{x} + (p_c - p)\delta p\}\, \mathrm{d}\Omega_0 \tag{70}$$

where [Dev] is the deviatoric projection operator and p_c is the constitutive Kirchhoff pressure, $p_c = \frac{1}{3}\mathrm{Tr}[\boldsymbol{\tau}]$. Integration is performed in the undeformed configuration (Ω_0) by using standard relations ($\boldsymbol{\tau} = \sigma J$). Note that if (70) is written in the deformed configuration, the classical definitions with the Cauchy stress are obtained.

Displacement and pressure interpolation are obtained as follows:

$$\boldsymbol{u}^h = \sum_{K=1}^{4} N_K(\boldsymbol{\xi})\boldsymbol{u}_K + N_5(\boldsymbol{\xi})\boldsymbol{u}_5 \tag{71}$$

$$p^h = \sum_{K=1}^{4} N_K(\boldsymbol{\xi})p_K \tag{72}$$

where

$$\begin{aligned} N_1(\boldsymbol{\xi}) &= \xi_1 \\ N_2(\boldsymbol{\xi}) &= \xi_2 \\ N_3(\boldsymbol{\xi}) &= \xi_3 \\ N_4(\boldsymbol{\xi}) &= 1 - \xi_1 - \xi_2 - \xi_3 \\ N_5(\boldsymbol{\xi}) &= \xi_1\xi_2\xi_3(1 - \xi_1 - \xi_2 - \xi_3) \end{aligned} \tag{73}$$

The mixed formulation presented in these references is convergent. In addition, as depicted in the following section the error map of $\det \boldsymbol{C}_p^{-1}$ is analyzed.

3 Assessment of errors in stress and incompressibility satisfaction

A seminal discussion of discrete constitutive equations and inequalities as non-smooth systems of Differential-Algebraic Equations (DAE) was presented by Ellsiepen and Hartmann in [29]. The Multilevel-Newton method was adopted with a local error estimator controlling the step size. Under that perspective, isoerror maps are now relegated to an illustrative tool of inspection of specific load paths.

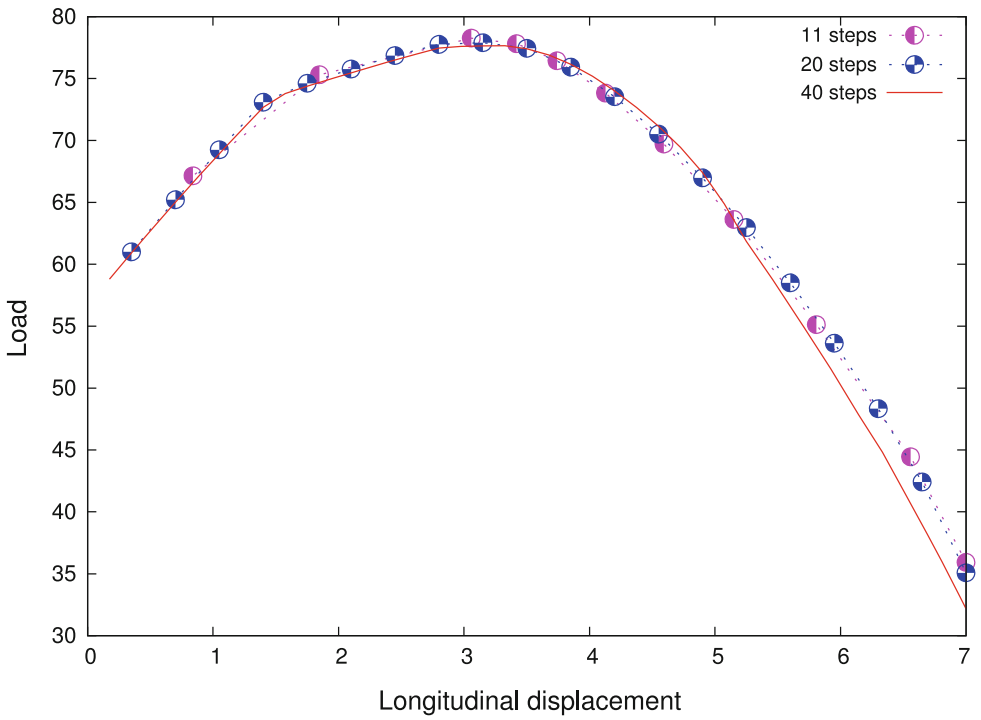

Fig. 8 Effect of the step size in the results of the von-Mises criterion (without projection) for the tension test

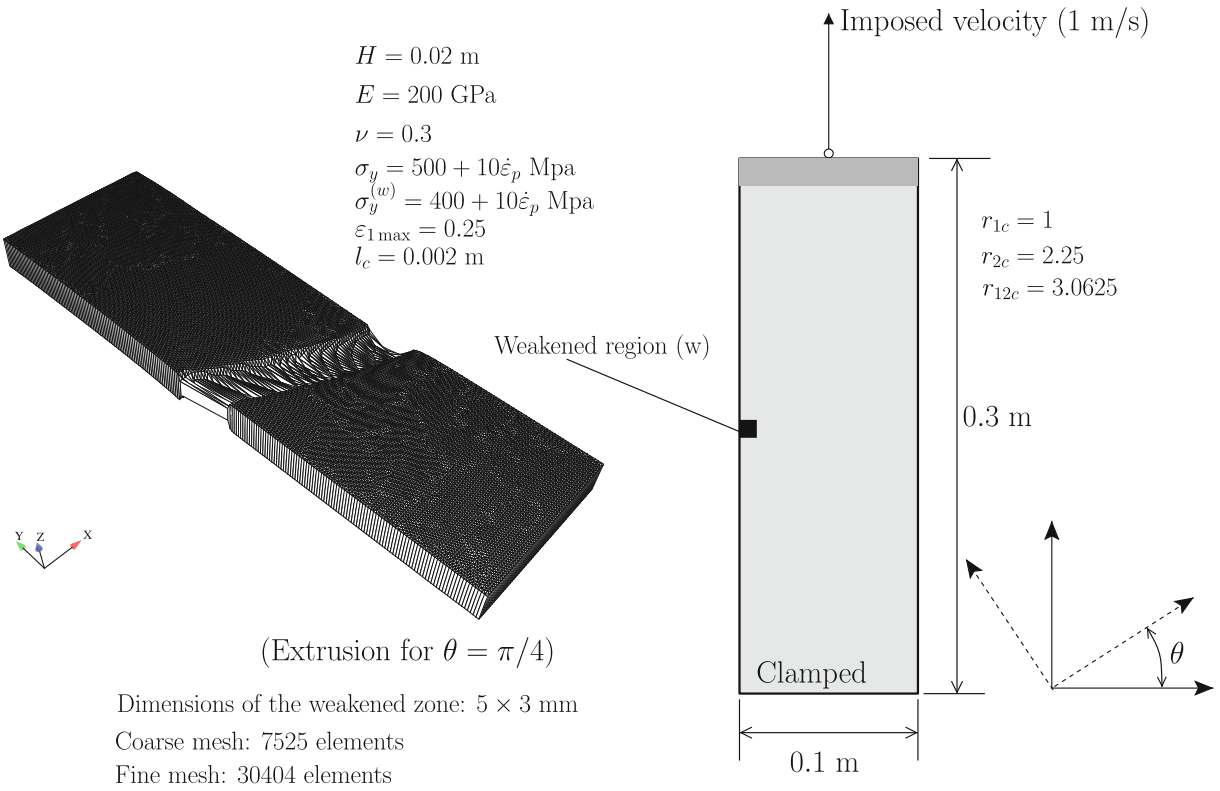

Fig. 9 Necking of a bar: relevant dimensions, loads and boundary conditions, and material properties. The characteristic length l_c is required to properly model the softening response

Isoerror maps (cf. [55]) are *extended* to finite strain plasticity and employed here to represent the error resulting from the time integration of:

- The plastic strain rate, $\boldsymbol{d}_p$ which is semi-implicit.
- The flow rule in terms of $\boldsymbol{b}_e$ which is fully implicit.

We also verify the accuracy of the incompressibility condition and the thickness variation error. In summary, the following quantities are inspected:

$$ERR_{\tau} = \frac{\|\boldsymbol{\tau} - \boldsymbol{\tau}_{100}\|_2}{\|\boldsymbol{\tau}_{100}\|_2} \tag{74}$$

$$ERR_{\det \boldsymbol{C}_p^{-1}} = \frac{\det \boldsymbol{b}_e - (\det \boldsymbol{F})^2}{(\det \boldsymbol{F})^2} \tag{75}$$

$$ERR_{\text{thickness}} = \frac{h - h_{100}}{h_{100}} \tag{76}$$

where the subscript 100 indicates that 100 steps were adopted to estimate the exact solution. It is worth noting that, although being the focus of many papers in the last century, incompressibility is *approximately* satisfied, with error values similar to those of stress and thickness. The quasi-incompressible Neo-Hookean model is adopted for the elastic behavior. Although neither the yield function nor the incompressibility condition are exactly satisfied,[14] corners in the so-called non-smooth yield surfaces [60] are *exactly* represented, as Fig. 2 shows. Comparatively, the two von-Mises return-mapping algorithms of Simo (with [56,57] and, in principal directions, [58]) are also shown (Fig. 3) with larger values of errors of stress and determinant of $\boldsymbol{C}_p^{-1}$. In that sense, an exact methodology for plastic incompressibility was presented by Hartmann et al. [31].

In addition, an assessment of the smoothing procedure is performed in 1D for the strain energy density of the nearly-incompressible Neo-Hookean model. For a pure one-step loading the effect of the error parameter is shown in Fig. 4. The problem is non-smooth for Error $= 0$ and otherwise smooth. In the examples, we adopt a default value of Error $= 1 \times 10^{-3}$.

4 Numerical examples

4.1 Tension test of a truncated cone: comparison of von-Mises and Tresca criteria

4.1.1 Classical testing and comparison with published results

We perform a test of a nearly-cylindrical specimen made of ASTM A-533 steel. It is subject to an imposed displacement in its base. This specific geometry is used to force necking

[14] Without smoothing of the complementarity condition, ERR_{τ} can also be significant.

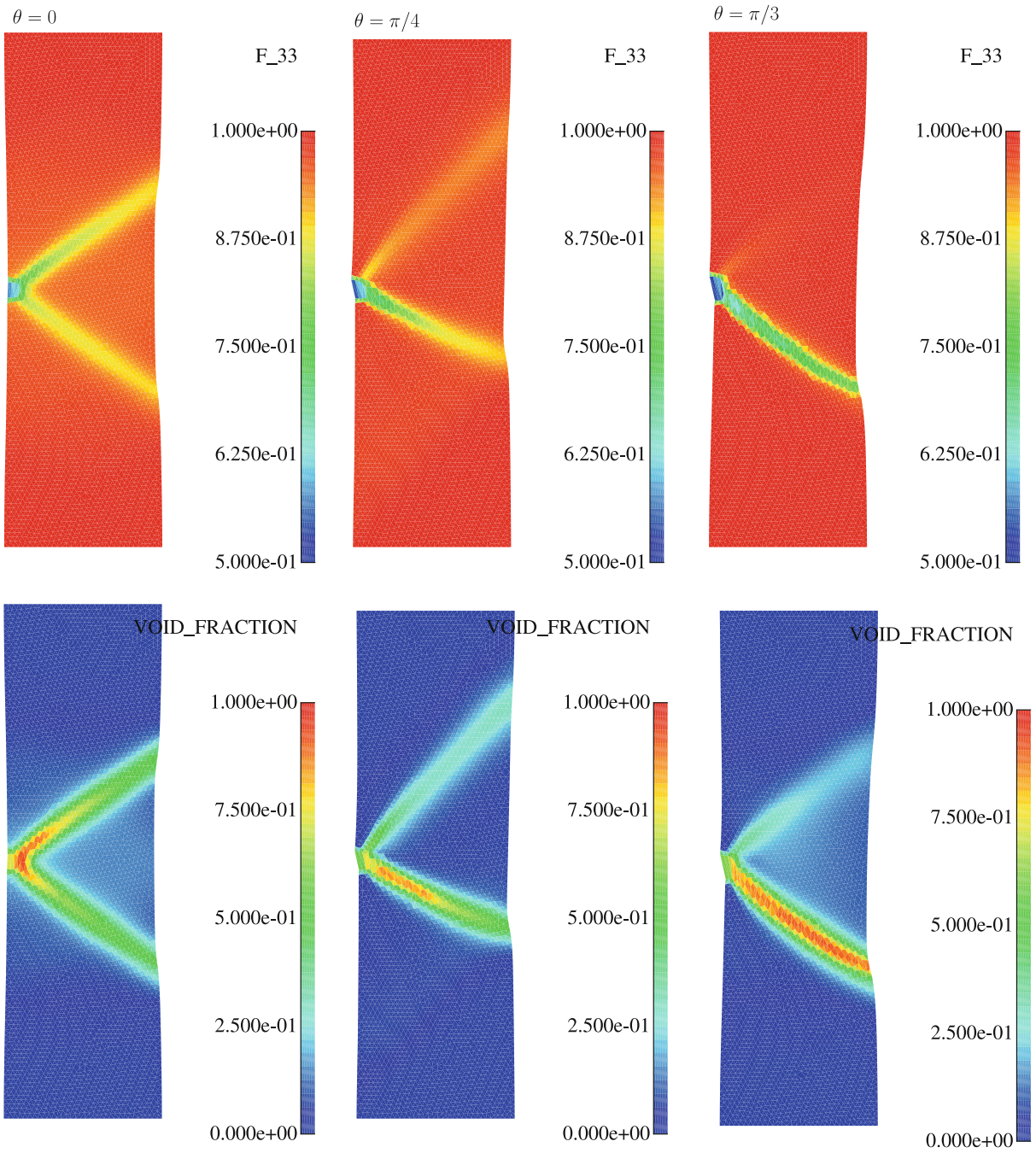

Fig. 10 Anisotropic plate: contour plots ($\theta = 0, \theta = \frac{\pi}{4}$ and $\theta = \frac{\pi}{3}$) for the void fraction and F_{33}. The coarse mesh is used. Localization angle should be $\pm 41.16°$ (cf. [43])

and was adopted by Simo [58] (see also Ref. [61] where the test is repeated) in the context of plasticity in principal components, where radial return is still applicable. The test data was obtained by Norris et al. [51] who performed an experimental test and used a 2D finite-difference simulation with grid rezoning in the specimen core. We use the properties of their specimen 2499R and a piece-wise linear law adapted from the one by Simo [58] and, in a axisymmetric version, by Peric and de Souza Neto [52]. The latter Authors performed the numerical test with Tresca criterion. Finite element simulations based on a finite-strain version of the radial-return algorithm result in convergence problems after the limit point is reached (cf. [64, pp. 358–359]). The geometry, boundary conditions and material properties are summarized in Fig. 5. The Neo-Hookean elastic model was used combined with the element presented in Sect. 2.9.

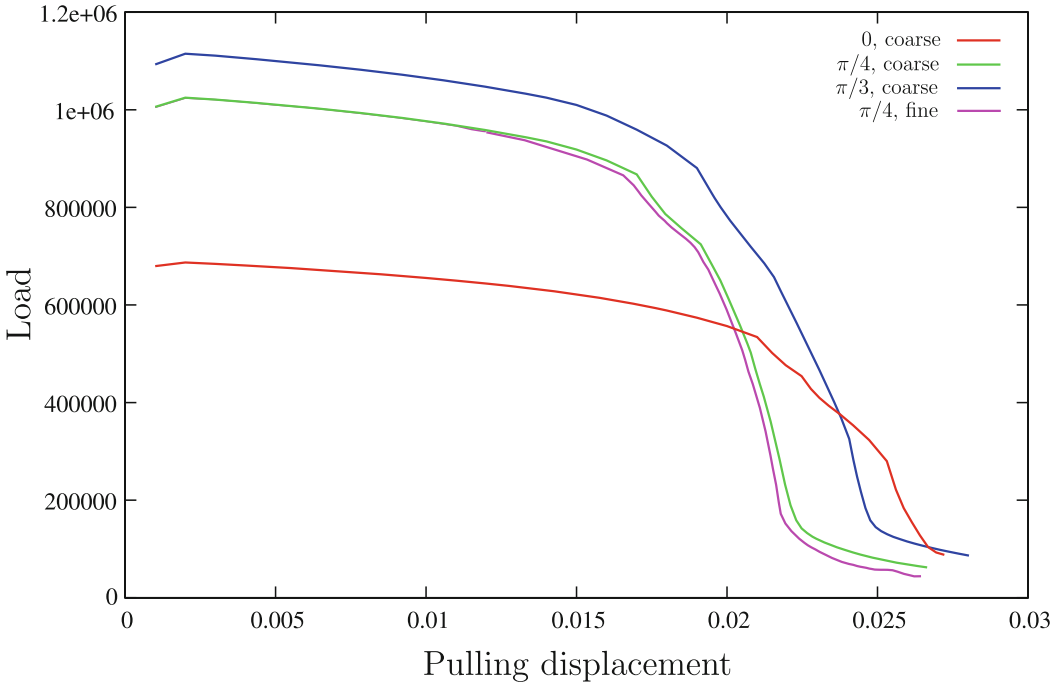

Fig. 11 Pulling displacement versus

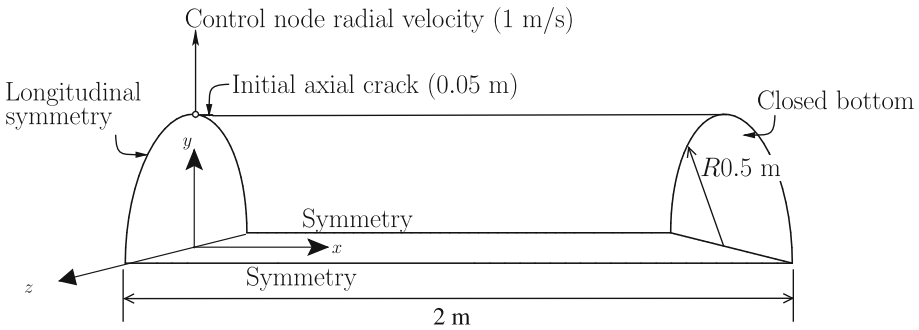

Fig. 12 Cylindrical shell: relevant dimensions, loads, boundary conditions and material properties

H (cylindrical surface)=0.025 m
H (bottom)=0.08 m
$f_{\text{crit}} = 0.2$
$E = 200$ GPa
$\nu = 0.3$
$\sigma_y = 500 + 2500\varepsilon_p + 0.015\dot{\varepsilon}_p$ MPa
$l_c = 0.1$ m
$\varepsilon_{1\,\max} = 0.05$

The effective plastic strain contour plots are shown in Fig. 6 for the two criteria. Note that the highly deformed elements near the core of the specimen were also obtained in Ref. [52]. The ductile damage model makes use of the following relations:

$$c_1 = 3\left(\frac{\sigma_{yc}}{\sigma_{yt}} - 1\right) \tag{77}$$

$$f = \max_{\text{history}}\left(\frac{\varepsilon_1}{\varepsilon_{1\,\max}}\right)^2 \tag{78}$$

where σ_{yc} is the compressive yield stress (given by the hardening law) and σ_{yt} is the tensile yield stress (we take it in this example as 2/3 lower than σ_{yc}). The quadratic law for the void fraction, (78), is a function of the maximum tensile Almansi strain (ε_1) and the allowed tensile strain ($\varepsilon_{1\,\max}$) which is here taken as 2. Analogous laws were adopted recently in [12].

The load and longitudinal displacement results are shown in Fig. 7. The results for the von-Mises criterion agree closely with the principal direction approach by Simo (cf. [58]). For the Tresca criterion, our results are slightly softer than the ones of Ref. [52]. Concerning the effective plastic strain contour plot (see Fig. 6) and mesh behavior, the Tresca criterion produces very close results to those reported in [52].

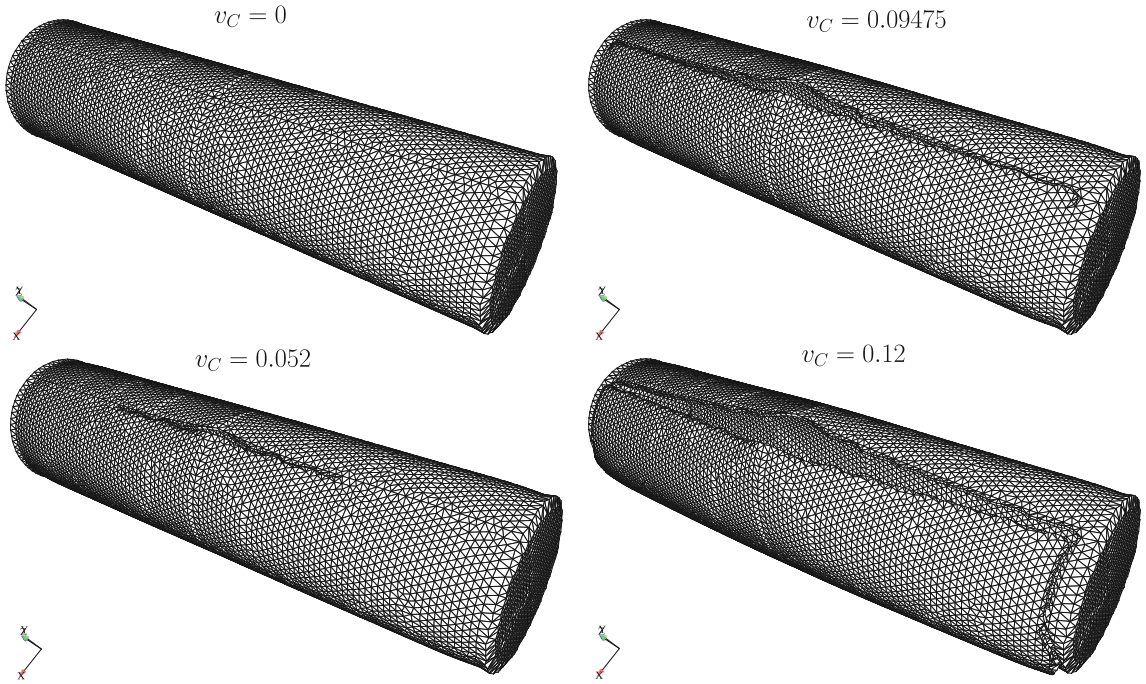

Fig. 13 Sequence of deformed meshes for the cylindrical shell problem (3894 × 4 elements)

4.1.2 Evaluation of step size effect

The prescribed number of displacement steps used to solve the tension test affects the load-longitudinal displacement results. In addition, this test is known to be very difficult to solve with large steps, since convergence difficulties are known to occur near the maximum load region (cf. [25]). Our method is veryrobust, as can be observed in Fig. 8. We can use only 11 steps (down from 15 steps in [7]) to simulate the process up to a longitudinal displacement of 7 consistent units (which agrees with the original simulation [58]). We are unaware of similar performance reported in the literature. In addition, since no artificial freeze of the flow vector is enforced, the results are very step-size insensitive. Specifically, the results using 11 steps are close to what is achieved with 40 steps. Some further localization is observed as diffuse necking is somehow sensitive to the number of steps (Table 3).

4.2 Plastic anisotropy testing (thickness variation) and diffuse necking

A finite strain plane-stress strip is tested in tension to verify the localization behavior of Hill criterion with three anisotropy angle: 0, $\pi/4$ and $\pi/3$ with the prototype ductile damage model. Thickness variation is accounted with the procedure described in Sect. 2.6. The geometry, boundary conditions and relevant properties are presented in Fig. 9. The test is inspired by the classical localization analysis (presented in the textbooks [16,43]). Results for the three values of θ are shown in Figs. 10 and 11. Contour plots are smooth and agree qualitatively with what is expected in the localization of an anisotropic damaged material. This further attests the robustness and generality of the proposed algorithms.

The load-displacement results are shown in Fig. 11 where a comparison between meshes is also performed for $\theta = \pi/4$.

4.3 Ductile fracture of a cylindrical shell

Combining our recent shell element with the ductile fracture algorithm recently presented ([11,12]) we are able to model implicitly ductile fracture of shells undergoing large strains. The data for our benchmark example is shown in Fig. 12 and it is formally introduced here. In addition, our recent shell element (cf. [10]) is adopted with the following parameters:

- 5 layers with 3 Gauss points each.
- 6 degrees-of-freedom in each node, including physically significant drilling rotation.
- Two scalar internal variables (void fraction f and effective plastic strain ε_p) are stored. In addition, the elastic left Cauchy-Green tensor is also stored.

It can be seen as a computational challenge to test the robustness of combined finite strain plasticity, ductile damage and fracture problems. We use damped linear control, an extension of our recently proposed control algorithm [8]. Two meshes are tested (and two planes of symmetry used): one containing 2218 elements and 1166 nodes and another containing 3894 elements and 2021 nodes. This type of problem

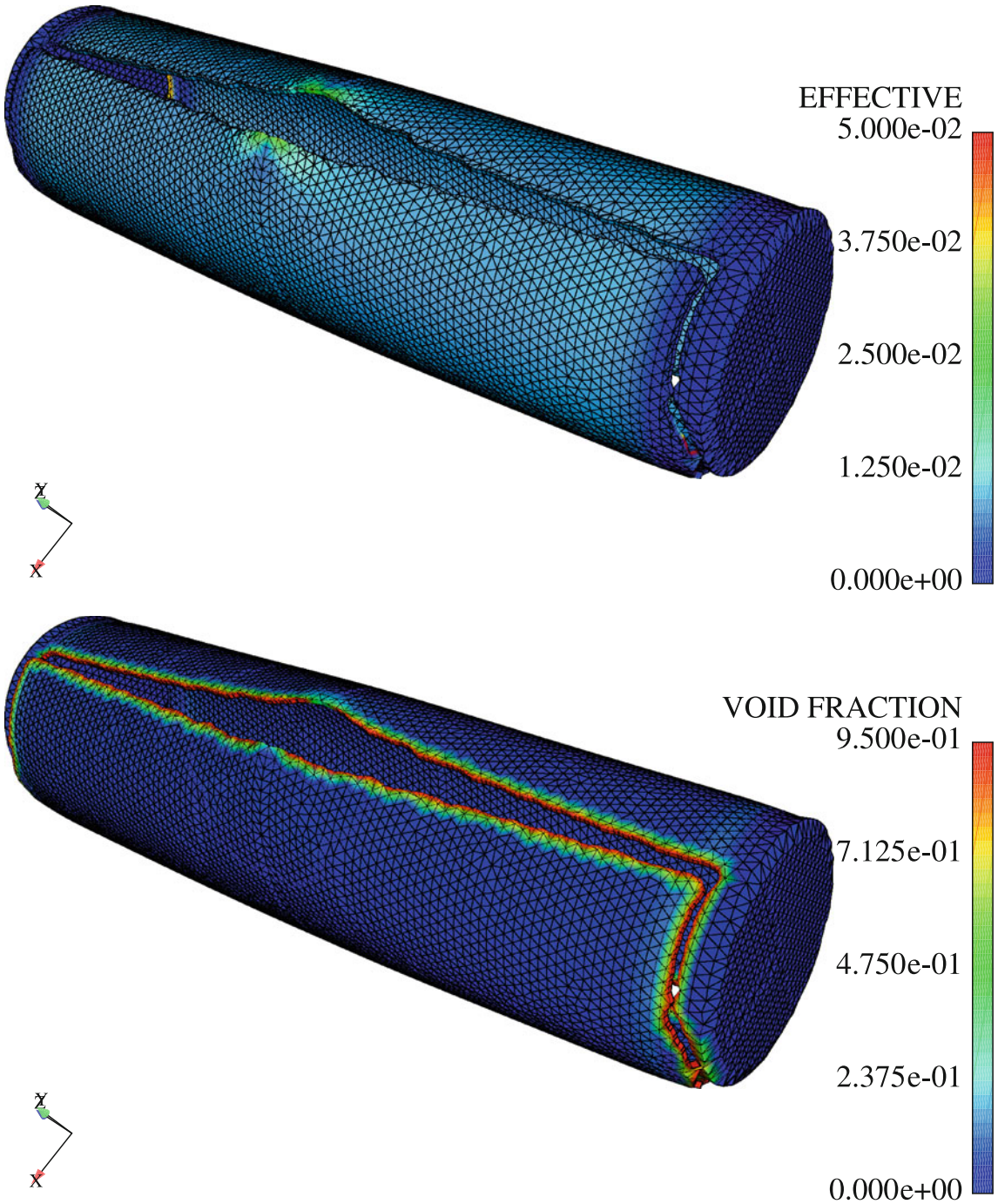

Fig. 14 Effective plastic strain contour plot and void fraction contour plot (3894 × 4 elements). Fractured elements have all integration points with 0.95 void fraction

demands a high degree of robustness to the elasto-plastic algorithm. Note that the crack path is determined by the Ma-Sutton criterion (cf. [47]) and there is no crack path *smoothing*. The crack nicely turns near the cylinder end, as can be observed in Fig. 13. Although experimental results are not available for this test, detonation tests (cf. [22]) of pipes produce very similar crack paths. Effective plastic strain and void fraction contour plots are shown in Fig. 14. Pressure-displacement results are presented in Fig. 15 where very good agreement between the two meshes can be observed.

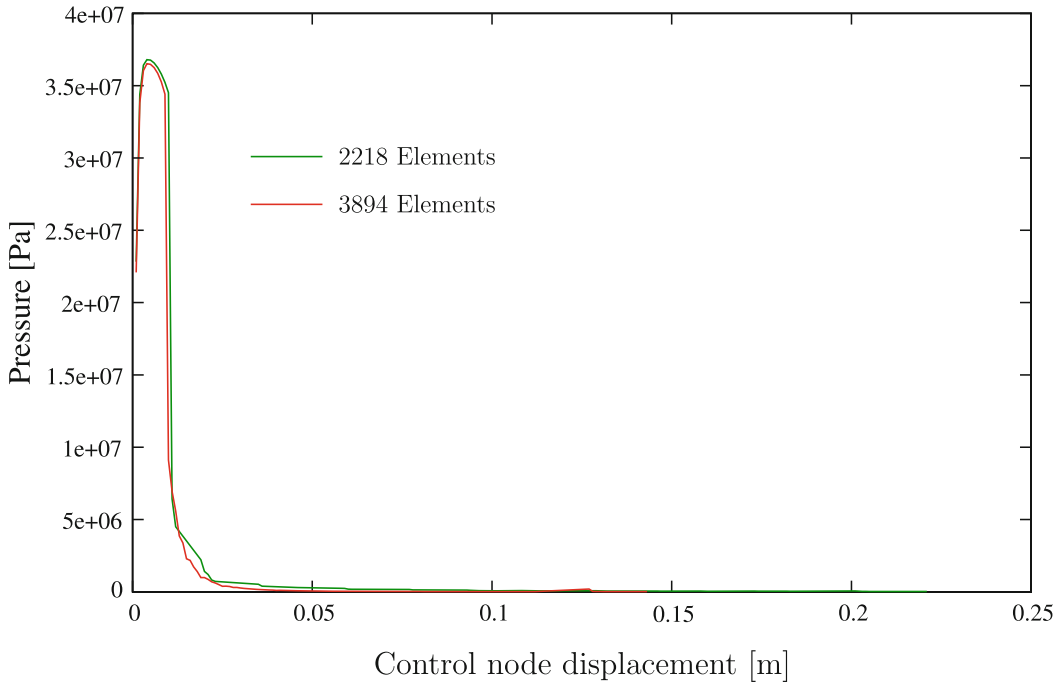

Fig. 15 Control node displacement versus internal pressure for the cracking cylinder

5 Conclusions

A general framework for finite strain plasticity appropriate for hyperelastic isotropic laws, plastic anisotropy and damage laws was presented. The flow rule is semi-implicitly integrated and the remaining constitutive equations are implicitly integrated. Smoothing by use of Chen-Mangasarian functions replaced the strict complementarity condition, so that the return-mapping algorithm was avoided. This was found to be specially relevant for ductile fracture examples, since they are very demanding in terms of convergence properties of elasto-plastic algorithms. Besides being able to solve the tension test benchmark with much fewer steps than before, additional examples included damage and plastic anisotropy. The overall scheme is computationally simpler than previous general integration schemes. It was found that computational costs are higher than classical J_2 Neo-Hookean based or Hencky-based approaches, but arbitrary isotropic elastic laws, flow rules, yield functions and hardening functions can be adopted. In addition, since no return-mapping is required, nor a particular solution method for plasticity, we can include more complex behavior without the effort usually required to derive closed-form quantities for specific return-mappings in finite strain plasticity.

Acknowledgments The authors gratefully acknowledge financing from the "Fundação para a Ciência e a Tecnologia" under the Project PTDC/EME-PME/108751 and the Program COMPETE FCOMP-01-0124-FEDER-010267. The first author is grateful to Professor Philipe Geubelle and Dr. Scot Breitenfeld (University of Illinois) for several discussions and support of SIMPLAS ([3]).

References

1. Antman SS (2005) Nonlinear problems of elasticity, 2nd edn. Springer, New York
2. Antman SS, Marlow RS (1991) Material constraints, lagrange multipliers, and compatibility. Arch Ration Mech Anal 116:257–299
3. Areias P (2011) Simplas. http://ssm7.ae.uiuc.edu:80/simplas
4. Areias P, Belytschko T (2006) Analysis of finite strain anisotropic elastoplastic fracture in thin plates and shells. J Aerosp Eng 19(4):259–270
5. Areias P, Matouš K (2008) Finite element formulation for modeling nonlinear viscoelastic elastomers. Comput Method Appl Mech Eng 197:4702–4717
6. Areias P, Matouš K (2008) Stabilized four-node tetrahedron with nonlocal pressure for modeling hyperelastic materials. Int J Numer Method Eng 76(8):1185–1201
7. Areias P, Rabczuk T (2010) Smooth finite strain plasticity with nonlocal pressure support. Int J Numer Method Eng 81:106–134
8. Areias P, Dias-da-Costa D, Alfaiate J, Júlio E (2009) Arbitrary bi-dimensional finite strain cohesive crack propagation. Comput Mech 45(1):61–75
9. Areias P, Ritto-Corrêa M, Martins JAC (2010) Finite strain plasticity, the stress condition and a complete shell model. Comput Mech 45:189–209
10. Areias P, Garção J, Pires EB, Infante Barbosa J (2011) Exact corotational shell for finite strains and fracture. Comput Mech 48:385–406
11. Areias P, Van Goethem N, Pires EB (2011) Constrained ale-based discrete fracture in shells with quasi-brittle and ductile materials. In: CFRAC 2011 international conference, Barcelona, Spain, CIMNE

12. Areias P, Van Goethem N, Pires EB (2011) A damage model for ductile crack initiation and propagation. Comput Mech 47(6): 641–656
13. Arnold DN, Brezzi F, Fortin M (1984) A stable finite element for the Stokes equations. Calcolo XXI(IV):337–344
14. Bathe K-J (1996) Finite element procedures. Prentice-Hall, Upper Saddle River
15. Belytschko T, Liu WK, Moran B (2000) Nonlinear finite elements for continua and structures. Wiley, New York
16. Besson J, Cailletaud G, Chaboche J-L, Forest S, Blétry M (2010) Non-linear mechanics of materials. Springer, New York
17. Bonet J, Wood RD (2008) Nonlinear continuum mechanics for finite element analysis, 2nd edn. Cambridge University Press, Cambridge
18. Brezzi F, Bathe K-J (1990) A discourse on the stability conditions for mixed finite element formulations. Comput Method Appl Mech Eng 82:27–57
19. Brezzi F, Fortin M (1991) Mixed and hybrid finite element methods. Springer, New York
20. Caminero MA, Montáns FJ, Bathe KJ (2011) Modeling large strain anisotropic elasto-plasticity with logarithmic strain and stress measures. Comput Struct 89:826–843
21. Chadwick P (1999) Continuum mechanics. Concise theory and problems, 2nd edn. Dover Publications, Mineola
22. Chao TW, Shepherd JE (2005) Fracture response of externally flawed aluminum cylindrical shells under internal gaseous detonation loading. Int J Fract 134:59–90
23. Chen C, Mangasarian OL (1995) Smoothing methods for convex inequalities and linear complementarity problems. Math Program 71(1):51–69
24. Chen C, Mangasarian OL (1996) A class of smoothing functions for nonlinear and mixed complementarity problems. Comput Optim Appl 5:97–138
25. Crisfield MA, Norris V (1999) A stabilized large-strain elastoplastic $Q_1 - P_0$ method. Int J Numer Method Eng 46:579–592
26. de Borst R (1987) Integration of plasticity equations for singular yield functions. Comput Struct 26(5):823–829
27. de Souza Neto EA (2004) On general isotropic tensor functions of one tensor. Int J Numer Method Eng 61:880–895
28. Dettmer W, Reese S (2004) On the theoretical and numerical modelling of Armstrong-Frederick kinematic hardening in the finite strain regime. Comput Method Appl Mech Eng 193:87–116
29. Ellsiepen P, Hartmann S (2001) Remarks on the interpretation of current non-linear finite-element-analyses as differential-algebraic equations. Int J Numer Method Eng 51:679–707
30. Hartmann S (2005) A remark on the application of the Newton–Raphson method in non-linear finite element analysis. Comput Mech 36(2):100–116
31. Hartmann S, Quint KJ, Arnold M (2008) On plastic incompressibility within time-adaptive finite elements combined with projection techniques. Comput Method Appl Mech Eng 198:178–193
32. He Q-C, Vallée C, Lerintiu C (2005) Explicit expressions for the plastic normality-flow rule associated to the tresca yield criterion. ZAMP Zeitschrift für angewandte Mathematik und Physik 56: 357–366
33. Holzapfel GA (2000) Nonlinear solid mechanics: a continuum approach for engineers. Wiley, New York
34. Hughes TJR, Winget J (1980) Finite rotation effects in numerical integration of rate constitutive equations arising in large-deformation analysis. Int J Numer Method Eng 15(12):1862–1867
35. Johansson G, Ekh M, Runesson K (2005) Computational modeling of inelastic large ratcheting strains. Int J Plast 21:955–980
36. Key SW, Krieg RD (1982) On the numerical implementation of inelastic time dependent and time independent, finite strain constitutive equations in structural mechanics. Comput Method Appl Mech Eng 33:439–452
37. Klinkel S, Govindjee S (2002) Using finite strain 3d-material models in beam and shell elements. Eng Comput 19(8):909–921
38. Klisinski M (1998) On constitutive equations for arbitrary stress–strain control in multi-surface plasticity. Int J Solids Struct 35(20):2655–2678
39. Korelc J (2002) Multi-language and multi-environment generation of nonlinear finite element codes. Eng Comput 18(4):312–327
40. Kulkarni DV, Tortorelli DA, Wallin M (2007) A Newton-Schur alternative to the consistent tangent approach in computational plasticity. Comput Method Appl Mech Eng 196:1169–1177
41. Lee EH (1969) Elasto-plastic deformation at finite strains. J Appl Mech ASME 36:1–6
42. Lee M-G, Kim JH, Ryou H, Chung K, Youn JR, Kang TJ (2006) Numerical implementation of modified Coulomb-Mohr yield criterion for anisotropic and asymmetric materials. Fiber Polym 7(3):276–285
43. Lemaitre J (1996) A course on damage mechanics, 2nd edn. Springer, New York
44. Lubliner J (1990) Plasticity theory. Macmillan, New York
45. Lührs G, Hartmann S, Haupt P (1997) On the numerical treatment of finite deformations in elastoviscoplasticity. Comput Method Appl Mech Eng 144:1–21
46. Lush AM, Weber G, Anand L (1989) An implicit time-integration procedure for a set of internal variable constitutive equations for isotropic elasto-viscoplasticity. Int J Plast 5:521–549
47. Ma F, Deng X, Sutton MA, Newman Jr JC (1999) Mixed-mode crack behavior. A CTOD-based mixed-mode fracture criterion. Number STP 1359. ASTM American Society for Testing and Materials, West Conshohocken, PA, pp 86–110
48. Miehe C, Schröder J (2001) A comparative study of stress update algorithms for rate-independent and rate-dependent crystal plasticity. Int J Numer Method Eng 50:273–298
49. Moran B, Ortiz M, Shih CF (1990) Formulation of implicit finite element methods for multiplicative finite deformation plasticity. Int J Numer Method Eng 29:483–514
50. Nemat-Nasser S (2004) Plasticity: a treatise on finite deformation of heterogeneous inelastic materials. Cambridge University Press, Cambridge
51. Norris DMJr, Moran B, Scudder JK, Quiñones DF (1978) A computer simulation of the tension test. J Mech Phys Solids 26:1–19
52. Perić D, de Souza Neto EA (1999) A new computational model for Tresca plasticity at finite strains with an optimal parametrization in the principal space. Comput Method Appl Mech Eng 171: 463–489
53. Rousselier G, Devaux J-C, Mottet G, Devesa G (1989) Nonlinear fracture mechanics: volume II—elastic–plastic fracture. A methodology for ductile fracture analysis based on damage mechanics: an illustration of a local approach of fracture. Number STP 995. American Society for Testing and Materials, Philadelphia, pp 332–354
54. Schmidt-Baldassari M (2003) Numerical concepts for rate-independent single crystal plasticity. Comput Method Appl Mech Eng 192:1261–1280
55. Schreyer HL, Kulak RL, Kramer JM (1979) Accurate numerical solutions for elasto-plastic models. J Press Vessel Technol 101: 226–334
56. Simo JC (1988) A framework for finite strain elastoplasticity based on maximum plastic dissipation and the multiplicative decomposition: part I. continuum formulation. Comput Method Appl Mech Eng 66:199–219
57. Simo JC (1988) A framework for finite strain elastoplasticity based on maximum plastic dissipation and the multiplicative decompo-

sition: part II. computational aspects. Comput Method Appl Mech Eng 68:1–31
58. Simo JC (1992) Algorithms for static and dynamic multiplicative plasticity that preserve the classical return mapping schemes of the infinitesimal theory. Comput Method Appl Mech Eng 99:61–112
59. Simo JC, Armero F (1992) Geometrically non-linear enhanced strain mixed methods and the method of incompatible modes. Int J Numer Method Eng 33:1413–1449
60. Simo JC, Hughes TJR (1998) Computational inelasticity. Interdisciplinary applied mathematics. Springer, New York
61. Simo JC, Armero F, Taylor RL (1993) Improved versions of assumed strain tri-linear elements for 3D finite deformation problems. Comput Method Appl Mech Eng 110:359–386
62. Truesdell C, Noll W (2004) The non-linear field theories of mechanics, 3rd edn. Springer, New York
63. Weber G, Anand L (1990) Finite deformation constitutive equations and a time integration procedure for isotropic, hyperelastic–viscoplastic solids. Comput Method Appl Mech Eng 79:173–202
64. Zienkiewicz OC, Taylor RL (2000) The finite element method, vol 2, 5th edn. Butterworth Heinemann, Oxford